IN-39
122404
P-49

NASA TECHNICAL MEMORANDUM 107677

EFFECTS OF CONSTRAINT ON CRACK GROWTH UNDER AIRCRAFT SPECTRUM LOADING

J. C. Newman, Jr.

SEPTEMBER 1992

(NASA-TM-107677) EFFECTS OF CONSTRAINT ON CRACK GROWTH UNDER AIRCRAFT SPECTRUM LOADING (NASA) 49 p

N92-34178

Unclas

G3/39 0122404

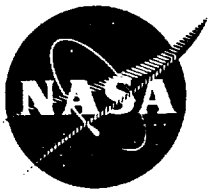

National Aeronautics and Space Administration

Langley Research Center
Hampton, Virginia 23665-5225

EFFECTS OF CONSTRAINT ON CRACK GROWTH UNDER AIRCRAFT SPECTRUM LOADING

J. C. Newman, Jr.
NASA Langley Research Center
Hampton, Virginia
USA

ABSTRACT

The objective of this paper is to study the effects of constraint on fatigue crack growth under aircraft spectrum loading. A plasticity-induced crack-closure model that accounts for constraint variations during the transition from flat-to-slant crack growth was used to correlate crack-growth rate data under constant-amplitude loading and to calculate crack growth under simulated aircraft spectrum loading. The model was applied to several thin-sheet aluminum alloy materials. Under laboratory air conditions, the transition was shown to be related to the size of the cyclic plastic zone based on the effective stress-intensity factor range for several sheet materials and thicknesses. Results from three-dimensional, elastic -plastic, finite-element analyses of a flat, straight-through crack in a thin-sheet aluminum alloy specimen showed a constraint loss similar to that assumed in the model. Using test data and the closure model, the location of the constraint-loss regime in terms of growth rate and the value of the constraint factor at these rates were determined by trial-and-error. The model was then used to calculate crack growth under the TWIST spectrum. The calculated results agreed reasonably well with test data. In general, the model predicted shorter crack-growth lives than tests under the TWIST spectrum by about 40 percent. For the TWIST spectrum clipped at Level III, the calculated lives were within about 20 percent. The results demonstrated that constraint variations, especially for thin-sheet alloys, should be accounted for to predict crack growth under typical aircraft spectra.

NOMENCLATURE

A_i	Coefficients in crack-opening stress equation
B	Specimen thickness, mm
c	Crack length, mm
c'	Crack length plus hole radius, mm
c_i	Initial crack length, mm
F	Boundary correction factor on stress-intensity factor
K	Applied stress-intensity factor, MPa-$\sqrt{m}$
N	Number of cycles
N_f	Number of cycles to failure
R	Stress ratio (S_{min}/S_{max})
r	Hole radius, mm
S	Applied stress, MPa
S_o	Crack-opening stress, MPa
S_o'	Crack-opening stress for extreme crack-growth rates, MPa
S_{max}	Maximum applied stress, MPa
S_{mf}	Mean flight stress, MPa
S_{min}	Minimum applied stress, MPa
w	Specimen half-width, mm
x,y,z	Cartesian coordinate system
α	Constraint factor on tensile yielding around crack front
α_g	Global constraint factor for yielded elements around crack front
ΔK	Stress-intensity factor range, MPa-$\sqrt{m}$
ΔK_{eff}	Effective stress-intensity factor range, MPa-$\sqrt{m}$
	range, MPa-$\sqrt{m}$
$(\Delta K_{eff})_T$	Effective stress-intensity factor at transition, MPa-$\sqrt{m}$
$(\Delta K_{eff})_{th}$	Effective stress-intensity factor threshold, MPa-$\sqrt{m}$

μ	Transitional coefficient
ρ	Plastic-zone size, mm
σ_o	Flow stress (average between σ_{ys} and σ_u), MPa
σ_{yy}	Normal stress acting in y-direction, MPa
σ_{ys}	Yield stress (0.2 percent offset), MPa
σ_u	Ultimate tensile strength, MPa
ω	Cyclic-plastic-zone size, mm

INTRODUCTION

In a review paper on the status of flight simulation fatigue crack growth predictive concepts, Wanhill and Schijve [1] discussed the short comings in the present technology and suggested some improvements. Several of the these improvements will be addressed in this paper. To predict crack growth under spectrum loading, fatigue crack growth data under constant-amplitude loading must be obtained over a large range of crack-growth rates from threshold to near fracture under cyclic loading conditions. Unfortunately, this type of data is not always available. This lack of data may be one of the reasons for some of the problems encountered in previous predictive models. Crack-growth rates under low and high stress ratios are also very important because the high stress ratio test data basically give the effective stress-intensity factor range [2], ΔK_{eff}, against crack-growth rate relation that is used in closure-based crack-growth models. The data at low and high stress ratios have also been used in the past to obtain a "constraint factor" to correlate constant-amplitude data over a wide range in stress ratios [3]. The constraint factor was introduced in the strip-yield closure model to account for crack-closure behavior under plane-stress or plane-strain conditions.

As pointed out by Yoder et.al. [4] and others, the stress-intensity factor range, ΔK, against crack-growth rate relationship for aluminum and titanium alloys do not follow a power law or sigmoidal shape but show sharp changes in slope or transitions at particular values of ΔK. These transitions, which are caused by microstructural features and are influenced by the environment, should be accounted for in the baseline ΔK_{eff}-rate relation. Fortunately, these transitions tend to occur at nearly the same crack-growth rates for various stress ratios and, thus, a unique ΔK_{eff}-rate relation is possible for some materials if a proper constraint factor has been selected.

As a crack grows in a finite body under cyclic loading (constant stress range), the plastic-zone size at the crack front increases. At low rates, plane-strain conditions should prevail but as the plastic-zone size becomes large compared to sheet thickness, a loss of constraint is expected. This constraint loss has been associated with the transition from flat-to-slant crack growth by many investigators (see for example, ref. 5). Numerous researchers have studied the transition from flat-to-slant crack growth or shear-lip development, as illustrated in Figure 1. Wilhem [6], Swanson et.al. [7] and Schijve [8] presented some experimental data on this behavior. Wilhem indicated that the beginning of the transition from flat-to-slant crack growth may be independent of sheet thickness. Swanson et.al. presented some data on the end of transition. The end of transition is usually easy to detect if the shear-mode fracture is on a 45 degree plane, as shown in Figure 1. However, when the shear mode develops into a double shear (or V-shaped profile), then the determination of the end of the transition is less distinct. Schijve also pointed out that the transition occurred at nearly the same crack-growth rate over a wide range in stress ratios for an aluminum alloy. Later, Schijve [9], using Elber's crack

closure concept, proposed that the transition should be controlled by ΔK_{eff}. These observations will be used herein to help select the constraint-loss regimes.

During fatigue crack growth rate tests, Elber [2] observed that fatigue-crack surfaces contact each other even during tension-tension cyclic loading. This observation and the exposition of the crack-closure phenomenon have explained many crack-growth characteristics, especially those under variable-amplitude loading. Since the discovery of plasticity-induced closure, several other closure mechanisms have been identified, such as roughness- and oxide-induced closure [10,11]. These developments have greatly improved our understanding of the complex interactions that occur during fatigue crack growth under variable-amplitude and spectrum loading [12,13]. Several numerical models of plasticity-induced closure (see ref. 1) have also been developed during the last fifteen years to calculate crack-closure behavior under aircraft spectrum loading.

The objective of this paper is to study the influence of constraint on fatigue crack growth under simulated aircraft spectrum loading using an analytical crack-closure model. The model [3,14] was used to correlate crack growth rate data under constant-amplitude loading and to calculate crack growth under the TWIST [15] standardized flight load spectra and various clipped versions. Several thin-sheet aluminum alloy materials were analyzed. The model, based on the Dugdale model [16], included a constraint factor that approximately accounts for the state-of-stress effects on plastic-zone development and on crack closure. This paper demonstrates how constraint plays a leading role in the retardation and acceleration effects that occur under aircraft spectrum loading. Under laboratory air conditions, the transition from flat-to-slant crack growth and crack-closure behavior was studied on several materials and thicknesses to help establish

the constraint-loss regime. Results from a three-dimensional, elastic-plastic, finite-element analysis of a flat, straight-through crack (stationary and growing) in a thin-sheet aluminum alloy specimen were used to numerically study the constraint-loss regime. These results were compared with the assumptions made in the closure model. Using experimental data and the closure model, the location of the constraint-loss regime in terms of crack-growth rate and the value of the constraint factor at these rates were determined by trial-and-error. The model was then used to calculate crack growth under the TWIST loading. Analyses were made on 2024-T3 and 7075-T6 aluminum alloy materials for various thicknesses and the results will be compared with experimental data. Some suggestions on test and analysis procedures to help determine the constraint-loss regime are proposed.

ANALYTICAL CRACK CLOSURE MODEL

The analytical crack-closure model [3,14] was developed for a central through crack in a finite-width specimen subjected to uniform applied stress. The model was later extended to a through crack emanating from a circular hole and applied to the growth of small cracks [5]. The model was based on the Dugdale model [16], but modified to leave plastically deformed material in the wake of the crack. A schematic of the model at the maximum and minimum applied stress is shown in Figures 2a and 2b, respectively. Here a crack is growing from a hole in an elastic body (Region 1). At the maximum applied stress, S_{max}, the material in the plastic zone, ρ, (Region 2) carries the stress, $\alpha\sigma_0$. The constraint factor, α, accounts for the influence of stress state on tensile yielding at the crack front. For plane-stress conditions, α is equal to unity (original Dugdale model); and for simulated plane-strain conditions, α is equal to 3. Although the strip-yield model does not model the correct yield-zone pattern for plane-strain

conditions, the model with a high constraint factor is able to produce crack-surface displacements and crack-opening stresses quite similar to those calculated from elastic-plastic finite-element analyses of crack growth and closure for a finite-thickness (B = 6 mm) plate [17]. Thus, the model may be useful in simulating crack growth in finite-thickness bodies. As the crack grows under cyclic loading, residual plastically deformed material (Region 3) is left on the crack surfaces. During unloading, these surfaces contact each other at the minimum applied stress, as shown in Figure 2b. The material in the plastic zone and along the contacting surfaces was assumed to yield at $-\sigma_0$. (In the original model, the contacting surfaces were assumed to reduce the effectiveness of the crack and reduce the constraint around the crack front. On the basis of three-dimensional finite-element analyses, however, this assumption may need to be studied further but this is beyond the scope of the present paper.) Using the contact stresses (Fig. 2b), the crack-opening stress is calculated.

The crack-opening stress is the applied stress level S at which the crack surfaces are fully open and is denoted as S'_0. The model is able to predict crack-opening stresses as a function of crack length and load history. The crack-opening stress is then used to calculate the effective stress-intensity factor range, ΔK_{eff} [2]. In turn, the crack-growth rate is calculated using a ΔK_{eff}-against-crack-growth-rate relation.

Effective Stress-Intensity Factor Range

Elber's effective stress-intensity factor range [2] was based on linear-elastic analyses and is given by

$$\Delta K_{eff} = (S_{max} - S'_0) \sqrt{\pi c}\, F \qquad (1)$$

where S_{max} is the maximum applied stress, S_0' is the crack-opening stress, c is the crack length and F is the usual boundary-correction factor which accounts for the influence of boundaries on the stress-intensity factor.

Constant-Amplitude Loading

In reference 18, crack-opening stress equations for constant-amplitude loading were developed from the analytical crack-closure model calculations for a center-crack tension specimen. These equations were fit to the results from the closure model and gave S_0 as a function of stress ratio (R), maximum stress level (S_{max}/σ_0) and the constraint factor (α). Recently, the model and equations were modified (see ref. 14) to account for extreme crack-growth rates, such as those under extremely high loads or proof testing, and is given by

$$S_0'/S_{max} = S_0/S_{max} + 0.3\ \sigma_0\ \sqrt{\Delta c/c}\ /(S_{max}F) \qquad (2)$$

where S_{max} is the maximum applied stress, σ_0 is the flow stress (average between the yield stress and ultimate tensile strength), Δc is the crack-growth increment (or rate per one cycle) and c is the current crack length. The boundary-correction factor, F, for the center-crack tension specimen was included to account for the influence of finite width. The crack-opening stress equations for S_0 will be presented later. Comparisons with the modified model [14] showed that equation 2 was reasonably accurate over a wide range in constant-amplitude loading conditions for S_{max}/σ_0 less than about 0.6. The difference between S_0' and S_0 was only significant (greater than a 2 percent effect on crack-opening stresses) for crack-growth rates greater than about 10^{-5} m/cycle. For $S_{max}/\sigma_0 > 0.6$, the crack-opening stresses should be calculated from the model.

The crack-opening stress equations for S_0 were originally developed by fitting to the calculated results from the model [18]. The equations will

be presented here because they have been slightly modified to include the effects of specimen width and their limits of application have been extended. The equations are

$$S_o/S_{max} = A_0 + A_1R + A_2R^2 + A_3R^3 \quad \text{for } R \geq 0 \tag{3}$$

and $$S_o/S_{max} = A_0 + A_1R \quad \text{for } R < 0 \tag{4}$$

where $R = S_{min}/S_{max}$, $S_{max}/\sigma_o < 0.8$, $S_{min}/\sigma_o > -1$, $S_o/S_{max} = R$ if S_o/S_{max} is less than R, and $S_o/S_{max} = 0$ if S_o/S_{max} is negative. The A_i coefficients are functions of α and S_{max}/σ_o and are given by:

$$\left.\begin{aligned} A_0 &= (0.825 - 0.34\alpha + 0.05\alpha^2)\,[\cos(\pi S_{max}F/2\sigma_o)]^{1/\alpha} \\ A_1 &= (0.415 - 0.071\alpha)\,S_{max}F/\sigma_o \\ A_2 &= 1 - A_0 - A_1 - A_3 \\ A_3 &= 2A_0 + A_1 - 1 \end{aligned}\right\} \tag{5}$$

for $\alpha = 1$ to 3. Again, the boundary-correction factor, F, was added to these equations to account for the influence of finite width on crack-opening stresses. These equations are used to correlate fatigue crack-growth rate data from center-crack tension specimens to obtain effective stress-intensity factor range against crack-growth rate relations. (Reference 14 also shows how equations 1-5 can be applied to standard compact tension specimens.)

Equations 2-5 give approximate crack-opening stress equations that agree fairly well with the results from the modified closure model [14]. A comparison between the equations and the model for a crack in an infinite body is shown in Figure 3. To severely test the equations, variable constraint (α = 2.4 for rates less than 1E-07 m/cycle and α = 1.2 for rates greater than 1E-06 m/cycle) was used. The solid curves show results from

the model for an R = 0.1 simulation at a high stress level. The crack-length-against-cycles results from the model were used to develop ΔK-rate data to be analyzed with the crack-opening stress equations, as if these data were from tests. The dashed curves show results from the equations. For constant α regions, the results from the equations agreed well with the model. Some differences were observed in the transition region between α = 2.4 to 1.2 because the equations were originally developed for steady-state constant-constraint conditions. From Figure 3, the maximum error in calculating ΔK_{eff} was 4 percent. The small vertical lines indicate the corresponding life ratio (N/N_f), in addition to indicating regions of constant constraint. (N is the number of cycles applied and N_f is the number of cycles required to fail the cracked body.)

Spectrum Loading

For variable-amplitude and spectrum loading, the crack-closure model must be used to compute the crack-opening stress history. Some typical crack-opening stresses under the TWIST load sequence for a crack in a center-crack-tension specimen are presented in this section. Comparisons are made for constant- and variable-constraint conditions.

In the first simulation, a constant constraint factor of 1.5 was selected. A crack length, c_i, of 1.5 mm in a 50 mm-wide specimen was selected as the initial condition. The solid lines in Figure 4 show crack-opening stresses calculated from the model as a function of the life ratio, N/N_f. (The dotted line denotes the zero level.) The crack-opening stresses have been normalized by S_{max} (maximum stress in the TWIST spectrum). Beyond a life ratio of about 0.1, the crack-opening stresses tended to oscillate about a mean value. The mean value is close to a damage-weighted average value [3], as shown by the dashed line. The damage-weighted average, $\bar{S}_0$,

value of 0.28 S_{max} was calculated during the second application of the TWIST spectrum. Using the constant crack-opening stress ($\bar{S}_0$) concept, the computed life to grow a crack from 1.5 mm in length to failure was 15 percent less than the life calculated from the complete model but the computer time was only about 0.3 of the time required to run the complete model. The constant crack-opening stress concept would be quite useful if a constant constraint factor could be used for the total life of a cracked component. For thick plates made of high-strength materials, a constant constraint factor may be satisfactory. However, as will be shown later, crack growth in thin-sheet aluminum alloy specimens under the TWIST spectrum cannot, in general, be modeled with a constant constraint factor.

Results from a crack-growth simulation using a variable-constraint condition that is closer to the actual behavior for thin-sheet aluminum alloys is shown in Figure 5. The constraint factor was assumed to change from $\alpha = 2$ to $\alpha = 1$ during the transitional region from flat-to-slant crack growth. Again, the calculated crack-opening stresses have been normalized by the maximum stress and are plotted against the life ratio. Under these conditions, the crack-opening stresses are steadily increasing as the crack grows while the constraint factor is dropping. Hereafter, the variable-constraint condition will be used to correlate constant-amplitude crack-growth rate data and to calculate crack growth under the TWIST spectrum loading.

TRANSITION FROM TENSILE-TO-SLANT CRACK GROWTH

As observed by Schijve [8], the end of transition from flat-to-slant crack growth, as shown in Figure 1, appeared to occur at the same fatigue crack-growth rate, independent of the stress ratio. Newman et.al. [5] used this observation to control the constraint-loss regime in the analytical

crack-closure model. Because the crack-closure concept is able to collapse crack-growth rate data onto nearly a single ΔK_{eff}-rate relation, Schijve [9] proposed that the effective stress-intensity factor should control the transition from flat-to-slant crack growth. To develop a simple method to estimate the transitional region, it is proposed that the transition occurs when the cyclic plastic-zone size calculated from the effective stress-intensity factor range at transition $(\Delta K_{eff})_T$ is a certain percentage of the sheet thickness. This relation is then given by

$$\mu = (\Delta K_{eff})_T/(\sigma_o \sqrt{B}) \tag{6}$$

where σ_o is the flow stress, B is the sheet thickness and μ is defined as the transitional coefficient. The $(\Delta K_{eff})_T$ is calculated from equations 1-5 assuming that the constraint at transition (fully 45 degree slant) was 1.1 (see the finite-element results in the next section). Using transitional data from the literature and some additional data generated in the present study under laboratory air conditions, the transitional coefficient (μ) is plotted against sheet thickness in Figure 6. Although considerable scatter is evident in the data, the general trend is for μ to be about 0.5 within ±20 percent for 1 to 6 mm-thick material. There is a slight trend, however, for μ to be lower for larger thicknesses. For thicknesses less than 2 mm, all values are higher than 0.5 and for thicknesses greater than 2.5 mm, nearly all values are lower than 0.5.

An interesting observation in Figure 6 is that a wide variety of materials (aluminum alloys, titanium alloys and high-strength steel) produce nearly the same μ value. These results, however, should only be applied to laboratory air tests. Previous studies by Schijve et.al. [24] and Vogelesang [20] have shown that the transition is strongly influenced by environment and frequency. They found that more aggressive environments

delayed the onset of transition to higher ΔK values. Further study is required to determine whether the constraint-loss regime, as used in this paper, under aggressive environments will still roughly correspond to the flat-to-slant crack-growth regime.

Whereas the ΔK_{eff} at the end of transition is a function of specimen thickness (eqn. 6), Wilhem [6] suggested that the beginning of shear-lip development for aluminum and titanium alloys may be independent of specimen thickness (1 to 6 mm thick). This is reasonable considering that the material at the free surface is in a state of plane stress, regardless of thickness. Furthermore, shear-lip formation should occur at nearly the same ΔK_{eff}. Thus, the beginning of the constraint-loss regime will be assumed to be independent of thickness for the materials and sheet thicknesses considered in this paper.

THREE-DIMENSIONAL FINITE-ELEMENT ANALYSIS

In a related effort to study constraint variations for aluminum alloy specimens using a three-dimensional, elastic-plastic, finite-element analysis [25], some results from that study are included here to help resolve the constraint-loss issue. The finite-element code, ZIP3D [26], was used to analyze center-crack-tension specimens made of an aluminum alloy material with an elastic-perfectly-plastic stress-strain behavior. The analyses were conducted on various thicknesses (B = 1.25 to 20 mm) with a half-width, w, of 40 mm and a c/w ratio of about 0.5 (see Fig. 1). The crack front, however, was flat and straight-through the thickness. The finite-element model (one-eighth of the specimen) had six layers through the half-thickness with the layer on the centerline of the specimen (Layer 1) being 0.15 B and the layer on the free surface (Layer 6) being 0.025 B. The smallest element size around the crack front was about 0.03 mm. The number of elements was 5706 and the number of nodes was 7203.

The finite-element model of the specimen was subjected to either monotonic or cyclic loading. Under monotonic loading, the crack front was held stationary but under cyclic loading the crack front extended one element size at the maximum applied stress during each cycle (for 5 cycles). Under monotonic loading, the specimens were loaded until the plastic zone extended across the net section. The computations for each specimen required about 2 hours on a super-computer.

Figure 7 shows the normal stress distribution, σ_{yy}, near the crack front ($x/c = 1$) for various layers through the thickness of the specimen. The specimen had a thickness of 2.5 mm and was subjected to an applied stress-intensity factor (K) level of $0.3\ \sigma_0\sqrt{w}$. The specimen developed a large amount of constraint (high σ_{yy}/σ_0) along the centerline (Layer 1) but constraint dropped rapidly near the free surface (Layer 6). A global constraint factor, α_g, was defined as the volume-weighted average of the ratio of σ_{yy}/σ_0 for all yielded elements along the crack plane ($y = 0$ and $x > c$). The α_g value is shown by the dashed line. Because the modified Dugdale model can only use a constant flow stress in the plastic zone, $\alpha_g\sigma_0$ may be an appropriate stress to use. Reference 17 has shown in a comparison of finite-element analyses and the modified Dugdale model under nearly plane-strain conditions ($\alpha = 1.73$) that the model with a constant flow stress gives reasonable crack-surface displacements and crack-opening stresses.

A comparison of α_g for monotonic and cyclic loading is shown in Figure 8 as a function of the applied K level. The solid curve shows the numerical results of monotonic loading with a stationary crack front. Results shown by the dashed curve at low K values were considered invalid because less than five elements were yielding at the crack front. The solid symbols show

numerical results from cyclic loading with crack extension at these particular K levels. The monotonic and cyclic loading results were in reasonable agreement with each other. These results show that the global constraint factor drops as the applied K level is increased (plastic-zone size increases) and approaches a value of about 1.1. The dashed-dot lines show the constraint variations that were assumed for a 3.1 mm-thick 2024-T3 Alclad material at R = 0 conditions. This assumed constraint variation is used later in the closure model to calculate crack growth under the TWIST spectrum. Although the transitions in the assumed constraint behavior are identified with the flat and shear mode transitional points (small vertical lines), in practice, the transitional points used in the closure model analysis may not necessarily correspond exactly with the actual transitional points on the test specimen. The experimental transitional behavior is only used as a guide in helping to select the constraint-loss regime. In this paper, the constraint-loss regime is found by trial-and-error to fit experimental crack-growth rate data under both constant-amplitude and spectrum loading. However, it is encouraging that the present numerical constraint-loss behavior and those required to fit experimental (crack length against flight) data are in fair agreement. Further numerical and experimental studies are necessary to resolve these issues.

EXPERIMENTAL AND CALCULATED FATIGUE CRACK GROWTH

In the following sections, fatigue crack growth rate data for 2024-T3 and 7075-T6 aluminum alloy materials under constant-amplitude loading will be correlated on the basis of ΔK_{eff}. These data cover a wide range in stress ratio but the thicknesses were about the same (B = 2 to 2.3 mm). The ΔK_{eff}-rate relations will then be used to calculate crack growth under the TWIST spectrum loading for the same materials but for thicknesses ranging from 1.6 to 3.1 mm. Because data were not available on the other

thicknesses, the ΔK_{eff}-rate relation determined from the 2 mm-thick materials were used for the 1.6 to 3.1 mm-thick materials. However, the location of the constraint-loss regime were adjusted to help fit the experimental (crack length against flight) data on some of the test.

Constant-Amplitude Loading

Aluminum Alloy 2024-T3 Bare.-The fatigue crack growth rate data obtained on bare 2024-T3 aluminum alloy [27,28] is shown in Figure 9. On the basis of ΔK_{eff}, the data collapsed into a narrow band with several changes in slope occurring at about the same crack-growth rate for all stress ratios. Some differences were observed in the threshold regime for rates lower than about 2E-09 m/cycle. For these calculations, a constraint factor (α) of 2 (nearly equivalent to Irwin's plane-strain condition, α = 1.73) was selected for rates less than 1E-07 m/cycle and α equal to 1 was selected for rates greater than 1E-06 m/cycle. For intermediate rates, α was varied linearly with the logarithm of crack-growth rate. The value of α = 2 was selected to collapse the various R-ratio data onto nearly a single ΔK_{eff}-rate curve. At high rates, it is expected that nearly plane-stress conditions should prevail and a low value of α was selected.

The location of the constraint-loss regime in terms of rate was selected to approximately match the transitional region from flat-to-slant crack growth. The solid symbols (see upper left-hand portion of figure) denote measured rates at the end of transition. (Note that the location of the constraint-loss regime and the transitional rates are plotted along the rate axis for convenience.) Although the location of the constraint-loss regime in term of rates and the values of α at these rates were selected by trial-and-error, they are consistent with global constraint values calculated from the finite-element analyses. Note, again, that the transitional points in the tests do not match the transitional points

selected for the constraint-loss regime. The loss of constraint is not abrupt but gradually approaches a value near unity. Because the model is only an approximation, these transitional points are not expected to match.

In the low crack-growth rate regime, near and at threshold, some tests and analyses have indicated that the threshold develops because of a rise in the crack-opening-stress-to-maximum-stress ratio (see ref. 29). This rise in crack-opening stress may be caused by oxide accumulation and the load-shedding procedure. In the threshold regime then, the actual ΔK_{eff}-rate data should lie at lower values of ΔK_{eff} because the rise in crack-opening stress was not accounted for in the current analysis. For the present study, an estimate was made for this behavior (based on small-crack data [5]) and it is shown by the solid line below rates of about 2E-09 m/cycle. A $(\Delta K_{eff})_{th}$ threshold was selected as 1.05 MPa-$\sqrt{m}$, again, on the basis of small-crack data. The baseline relation shown by the solid line is used in tabular form so that the sharp changes in slope can be modeled.

Aluminum Alloy 2024-T3 Alclad.-Figure 10 shows the crack-growth rate data for 2024-T3 Alclad aluminum alloy material [30]. These data again cover a wide range in stress ratio and the data correlated quite well with the same constraint factors as used for the bare material. The dashed curve is the ΔK_{eff}-rate relation obtained from the bare material. For most of the data, the clad and bare results agreed quite well. Depending upon the clad thickness, however, one would have expected to see a crack in the clad material grow slightly faster than that in the bare material because the core material is carrying a slightly higher stress-intensity factor.

The solid symbols again denote measured rates at the end of transition from flat-to-slant crack growth. The rates at transition were slightly lower than those measured on the bare material and may be caused by a combination of a slightly lower strength and smaller thickness, as indicated

by equation 6. The $(\Delta K_{eff})_T$ at transition was about 9 MPa-$\sqrt{m}$ and was determined from the ΔK_{eff}-rate relation at the transitional rate. For rates lower than 1E-08 m/cycle, the results from the bare material were used to estimate the baseline data for the clad alloy. In the bare material, a rapid change in slope was found at about 1E-08 m/cycle (see Fig. 9). Whether the clad alloy would show the same trend requires additional testing at lower rates. The baseline relation (solid curve) will be used later to calculate crack-growth rates under the TWIST spectrum and is given in tabular form in Table 1. The crack-growth rates and α for the assumed constraint-loss regime is given in Table 2.

Aluminum Alloy 7075-T6 Clad.-The ΔK_{eff}-rate relations for 7075-T6 aluminum alloy data from center-crack tension specimens are shown in Figure 11. The symbols show crack-growth rate data on a 7075-T6 Clad alloy [30,31]. (The LC9cs Clad alloy [32] had nearly the same chemical composition as 7075 but had a clad layer of about 90 μm.) These data show sharp changes in slope in the region near the transition from flat-to-slant crack growth. The 7075 clad and Lc9cs clad data agreed quite well and, as expected, cracks grew slightly faster in the clad alloys than in the bare. At high rates, the 7075 clad and bare data fell together. The solid symbols show measured rates at the end of transition for both the clad and bare alloys. Using the $(\Delta K_{eff})_T$ for the 2024-T3 Alclad material, an estimate for $(\Delta K_{eff})_T$ for the 7075-T6 Clad can be made by using equation 6. Assuming that μ is constant, the ratio of ΔK_{eff} values at transition should be equal to the ratio of flow stresses since they have the same thickness. Thus, the $(\Delta K_{eff})_T$ value for the 7075 material is about 11.1 MPa-$\sqrt{m}$ which gives a rate of about 1.2E-06 m/cycle. This value is in reasonable agreement with the experimental measurements. The location of the constraint-loss regime was also estimated on the basis of equation 6. A value of α = 1.15 was needed

because a constraint factor of unity gave too much delay under the TWIST spectrum, as will be discussed later. Because data was not available at low rates, the baseline relation (solid curve) for the clad material was faired between the clad and bare material relations [32] for rates lower than 1E-07 m/cycle. The baseline relation and constraint-loss regime (given in Table 1 and 2) will be used later to calculate crack-growth rates under the TWIST spectrum.

TWIST Spectrum Loading

As pointed out by Wanhill and Schijve [1], the ability to predict crack-growth behavior under the TWIST spectrum loading has eluded the empirical crack-growth (retardation and acceleration) models in the literature. However, the strip-yield models, such as those developed by Dill and Saff [33], Fuhring and Seeger [34], Newman [3], and de Koning and Liefting [35] probably have a reasonable chance of predicting such behavior. These models have numerical "memory" to account for the occurrence of overloads, underloads and overlapping plastic zones and should be able to characterize the plastic-deformation histories generated under the TWIST spectrum. As will be presented later, the constraint factor plays a leading role in allowing the strip-yield model to predict the crack-opening stress history that develops under the TWIST spectrum. In the following sections, the closure model [3,14] is used with the baseline ΔK_{eff}-rate relations, previously determined, to calculate crack growth in 2024-T3 and 7075-T6 aluminum alloy sheet materials under the original and clipped versions of the TWIST spectrum.

The TWIST [15] spectrum is composed of 4,000 different flights (or 394,665 cycles) and 4,000 landings. Loading in the spectrum is characterized by the mean flight stress, S_{mf}. The gust loading is composed of ten different stress amplitude levels. Level I is the highest ($\pm 1.6 S_{mf}$)

and Level X is the lowest. TWIST is often used in a form where the peak stress amplitudes are clipped (or reduced) to match a specific level. The TWIST spectrum at Level I is the original spectrum history but the spectrum at Level III means that any gust amplitudes higher than Level III, such as Levels I and II, are clipped to match Level III.

Aluminum Alloy 2024-T3 Alclad.-Wanhill [36,37] conducted spectrum crack-growth tests on center-crack tension specimens made of 2024-T3 Alclad material in two thicknesses (B = 1.6 and 3.1 mm). Tests were conducted under the TWIST spectrum clipped at Levels I and III with S_{mf}= 70 MPa. The initial crack starter notch half-length was 3.5 mm. Comparisons are made between experimental and calculated crack length against flights for Level III; and experimental and calculated crack length against crack-growth rate for Levels I and III. The crack-growth rate, dc/dF, is the change in crack length with change in flights.

Crack-length-against-flight data on the 1.6 and 3.1 mm-thick specimens tested under the TWIST (Level III) loading are shown in Figures 12 and 13, respectively. Each figure shows results (symbols) from two separate specimens tested under identical conditions. The solid curve is the calculated results from the closure model with the variable-constraint condition (α = 2 to 1) using the baseline ΔK_{eff}-rate relation in Table 1. The corresponding constraint-loss regime for the respective thicknesses is given in Table 2. In Table 2, note that the rate at the beginning of the constraint-loss regime was assumed to the the same for all thicknesses (B = 1.6 to 3.1 mm). However, the end of the constraint-loss regime was estimated on the basis of equation 6. From equation 6, a thicker specimen made of the same material would exhibit a larger $(\Delta K_{eff})_T$ value and, consequently, a higher crack-growth rate. Using these constraint-loss regimes and the model, the calculated results agreed well with the tests

(within 15 percent). The large increases in crack length at certain flights in both the tests and analyses are caused by Flight A and B [15], the two most severe flights in TWIST.

To illustrate why the variable-constraint conditions are necessary, example calculations are made for constant constraint conditions of either α = 1 or 2 (dashed-dot curves). The model with a low constraint condition (α = 1) predicted slightly longer flights to a given crack length than the test data for the thin material but predicted much longer lives for the thick material. Conversely, the predicted results for the higher constraint condition (α = 2) greatly under-predicted the behavior for both thicknesses except in the early stages of growth. If the thin material had been tested at a lower mean-flight stress level than 70 MPa, it is expected that the lives would have fallen closer to the α = 2 curve much like the 3.1 mm-thick material because the higher constraint condition would have been activated during more of the life time.

Figures 14 and 15 show a comparison between experimental [36] and calculated results of crack length against dc/dF under the TWIST loading (Levels I and III) for the 1.6 and 3.1 mm-thick specimens, respectively. Again, two specimens were tested under each condition and the results are shown by the two different symbols. For both levels and thicknesses, the closure model was able to calculate the initial rates quite accurately (curves). Calculated results under Level III agreed with the test results over nearly the complete range of crack lengths. The oscillations in the measured and calculated rates are caused by rapid growth and retardations due to the severe flights in TWIST. The calculated results under Level I, however, began to deviate from the test results after a crack length of about 12 mm. The ratio of calculated life to test life from an initial crack length of 3.5 mm to failure was 0.61 for both thicknesses.

ProvoKluit [38] conducted spectrum tests on center-crack tension specimens made of 2 mm-thick 2024-T3 Alclad material. These tests were conducted under the TWIST spectrum for Levels II to V and the test results (symbols) are shown in Figure 16. The solid curves are the calculated results from the closure model with the variable-constraint condition using the baseline ΔK_{eff}-rate relation in Table 1. The corresponding constraint-loss regime is given in Table 2. The calculated results agreed reasonable well with the test data (within 25 percent) except for Level II. Here the analysis under-predicted the test results by about 53 percent. The reason for this discrepancy is not known but the results are consistent with the previous results for tests conducted at Level I (shown in Figs. 14 and 15). The tests at Levels I and II are showing more retardation than the analyses. Some possible reasons for the short calculated lives may be the accumulation of oxide and fretting debris in the crack-front region for long life tests or improper constraint factors. The debris would elevate crack-opening stresses and reduce the crack-growth rates. Because the model does not account for oxide- and fretting-debris-induced closure, the calculated lives would be less than the tests. The selection of the constraint-loss regime and the constraint values still need further study.

Aluminum Alloy 7075-T6 Clad.-ProvoKluit [38] also conducted spectrum tests on center-crack tension specimens made of 2 mm-thick 7075-T6 Clad alloy. These tests were conducted under the TWIST spectrum for Levels I to V. The test results (symbols) for Levels I and II are shown in Figure 17(a) and those for Levels III to V are shown in Figure 17(b). Again, the solid curves show the calculated results from the closure model with the variable-constraint condition. Table 1 and 2 gives the baseline data for this material. The calculated results, again, fell short of the test data (about 30 percent) for all spectrum clipping levels. These tests are interesting,

in that, only one sequence of the TWIST spectrum is required to break the specimens. Flight A is the most severe flight in the sequence and flight B is the second most severe. The initial rates calculated from the the model were in good agreement with the test data, but the calculated rates rapidly increased after about 1200 flights. A detailed study of the calculated rates from the spectrum revealed that the faster growth between 1200 and 1650 flights was caused by the rapid increase in the slope of the ΔK_{eff}-rate relation at about 1E-08 m/cycle. If the growth in this regime could have been delayed, then growth under spectrum levels III and IV may have been delayed long enough to experience Flight B and caused more retardation and, consequently, longer lives. Before a more detailed study on the clad alloy is made, more constant-amplitude data at lower rates should be obtained.

DISCUSSION ON CONSTRAINT-LOSS REGIME AND THE MODEL

The results presented in this paper suggest that the constraint-loss regime is important in predicting the complex interactions that occur under the TWIST spectrum loading. In the final analysis, the test data from the spectrum tests, as well as the constant-amplitude data, were used to help establish the constraint-loss regime and the values of constraint. To develop a more predictive method, test and analyses procedures need to be developed to more accurately determine the constraint factors. Constant-amplitude tests at different stress ratios are not sensitive enough to constraint variations to be used as a reliable test [39]. However, single-spike overload tests with varying magnitudes of overloads will activate the constraint-loss regime at different rates and allow one to more precisely determine this regime.

In regard to the closure model, the constraint effects that develop at the crack front under a closed crack, a "compressive" constraint factor, need to be studied further. The most reliable method would be to conduct

three-dimensional, elastic-plastic, finite-element analyses of crack growth and closure. Results from Chermahini et.al. [40] suggest that the compressive constraint factor should lie between -1 and -2. The strip-yield closure model could be modified to match these finite-element results. As previously mentioned, however, the prediction of shorter crack-growth lives than tests under the TWIST spectrum may have been caused by other forms of closure, such as oxide- or fretting-debris-induced closure. Further study is needed to determine whether these forms of closure are significant under spectrum loading. Further improvements in the model may be needed to predict the interactions between these other forms of closure, constraint and spectrum loading.

CONCLUDING REMARKS

A plasticity-induced crack-closure model was used to study the effects of constraint on fatigue crack growth under the TWIST standardized flight load spectra and various clipped versions. Several thin-sheet 2024-T3 and 7075-T6 (bare and clad) aluminum alloy materials were analyzed. In the model, the constraint-loss regime was associated with the flat-to-slant crack-growth region. For a wide variety of materials and thicknesses under laboratory air conditions, the transition from flat-to-slant crack growth was found to occur at nearly the same cyclic plastic-zone-size-to-thickness ratio based on the effective stress-intensity factor range. This relationship and transitional data were used to help establish the constraint-loss regime. Results from three-dimensional, elastic-plastic, finite-element analyses of a flat, straight-through crack in a thin-sheet aluminum alloy specimen showed a constraint loss similar to that assumed in the model.

Using experimental data and the closure model, the location of the constraint-loss regime in terms of crack-growth rate and the value of the

constraint factor at these rates were found by trial-and-error. The effective stress-intensity factor against crack-growth rate relationship and the model was used to calculate crack growth under the TWIST simulated aircraft spectrum loading. The calculated results agreed reasonably well with test data. The model, in general, predicted shorter crack-growth lives by about 40 percent for test conducted under the TWIST spectrum. For the TWIST spectrum clipped at Level III, the calculated lives were within about 20 percent of the test data. These results demonstrated that constraint variations, especially for thin-sheet alloys, should be accounted for to predict crack growth under typical aircraft spectra. Some suggestions on test and analysis procedures to help determine the constraint-loss regime were proposed.

ACKNOWLEDGEMENT

The author would like to take this opportunity to thank Mr. E. P. Phillips, Dr. D. S. Dawicke and Mr. R. A. Everett for their help in determining transitional data on several materials.

REFERENCES

[1] Wanhill, R. J. H. and Schijve, J., "Current Status of Flight Simulation Fatigue Crack Growth Concepts," NLR MP 88001 U, 1988.

[2] Elber, W., "The Significance of Fatigue Crack Closure," Damage Tolerance in Aircraft Structures, ASTM STP 486, 1971, pp. 230-242.

[3] Newman, J. C., Jr., "A Crack-Closure Model for Predicting Fatigue Crack Growth under Aircraft Spectrum Loading," Methods and Models for Predicting Fatigue Crack Growth under Random Loading, ASTM STP 748, 1981, pp. 53-84.

[4] Yoder, G. R., Cooley, L. A. and Crooker, T. W., "On Microstructural Control of Near-Threshold Fatigue Crack Growth in 7000-Series Aluminum Alloys," NRL Memorandum Report 4787, Naval Research Laboratory, 1982.

[5] Newman, J. C., Jr., Swain, M. H. and Phillips, E. P., "An Assessment of the Small-Crack Effect for 2024-T3 Aluminum Alloy," Small Fatigue Cracks, R. O. Ritchie and J. Lankford, eds., The Metallurgical Society of AIME, 1986.

[6] Wilhem, D. P., "Investigation of Cyclic Crack Growth Transitional Behavior," Fatigue Crack Propagation, ASTM STP 415, 1967, pp. 363-383.

[7] Swanson, S. R., Cicci, F. and Hoppe, W., "Crack Propagation in Clad 7079-T6 Aluminum Alloy Sheet under Constant and Random Amplitude Fatigue Loading," Fatigue Crack Propagation, ASTM STP 415, 1967, pp. 312-362.

[8] Schijve, J., "Significance of Fatigue Cracks in Micro-Range and Macro-Range," Fatigue Crack Propagation, ASTM STP 415, 1967, pp. 415-459.

[9] Schijve, J., "Shear Lips on Fatigue Fractures in Aluminum Alloy Sheet Material," Delft University of Technology, Report LR-287, Sept. 1979.

[10] Walker, N. and Beevers, C. J., "A Fatigue Crack Closure Mechanism in Titanium," Fatigue of Engineering Materials and Structures, Vol. 1, 1979, pp. 135-148.

[11] Suresh, S. and Ritchie, R. O., "A Geometric Model for Fatigue Crack Closure Induced by Fracture Surface Roughness," Metallurgical Transactions, Vol. 13A, 1982, pp. 1627-1631.

[12] Schijve, J., "Observations on the Prediction of Fatigue Crack Growth Propagation under Variable-Amplitude Loading," Fatigue Crack Growth under Spectrum Loading, ASTM STP 595, 1976, pp. 3-23.

[13] Schijve, J. "Fatigue Crack Closure: Observations and Technical Significance," Mechanics of Fatigue Crack Closure, ASTM STP 982, 1988, pp. 5-34.

[14] Newman, J. C., Jr., "FASTRAN II - A Fatigue Crack Growth Structural Analysis Program," NASA TM 104159, Feb. 1992.

[15] de Jonge, J. B., Schutz, D., Lowak, H. and Schijve, J., "A Standardized Load Sequence for Flight Simulation Tests on Transport Aircraft Wing Structures," LBF-Bericht FB-106, NLR TR 73029 U, March 1973.

[16] Dugdale, D. S., "Yielding of Steel Sheets Containing Slits," Journal of Mechanics and Physics of Solids, Vol. 8, No. 2, 1960, pp. 100-104.

[17] Blom, A. F., Wang, G. S. and Chermahini, R. G., "Comparison of Crack Closure Results Obtained by 3-D Elastic-Plastic FEM and Modified Dugdale Model," International Conference on Computer Aided Assessment and Control of Localized Damage, Portsmouth, England, June 26-28, 1990.

[18] Newman, J. C., Jr., "A Crack-Opening Stress Equation for Fatigue Crack Growth," International Journal of Fracture, Vol. 24, 1984, R131-R135.

[19] Misawa, H. and Schijve, J., "Fatigue Crack Growth in Aluminum Alloy Sheet Material under Constant-Amplitude and Simplified Flight-Simulation Loading," Delft University of Technology, Report LR-381, Feb. 1983.

[20] Vogelesang, L. B., "The Effect of Environment on the Transition from Tensile Mode to Shear Mode During Fatigue Crack Growth in Aluminum Alloys - A Model for Environmentally Assisted Crack Growth," Delft University of Technology, Report LR-286, Oct. 1979.

[21] Zuidema, J. and Blaauw, H. S., "Slant Fatigue Crack Growth in Al 2024 Sheet Material," Engineering Fracture Mechanics, Vol. 29, 1988, pp. 401-413.

[22] Hudson, C. M., "Investigation of Fatigue Crack Growth in Ti-8Al-1Mo-1V (Duplex-Annealed) Specimens Having Various Widths," NASA TN D-3879, March 1967.

[23] Swain, M. H., Everett, R. A., Newman, J. C., Jr. and Phillips, E. P.,"The Growth of Short Cracks in 4340 Steel and Aluminum-Lithium 2090", Short-Crack Growth Behaviour in Various Aircraft Materials, AGARD Report No. 767, 1990, pp. 7.1-7.30.

[24] Schijve, J., Jacobs, F. A. and Tromp, P. J., "Environmental Effects on Crack Growth in Flight-Simulation Tests on 2024-T3 and 7075-T6 Material," NLR-TR 76104 U, National Aerospace Laboratory, 1976.

[25] Newman, J. C., Jr., Bigelow, C. A. and Shivakumar, K. N., "Three-Dimensional Elastic-Plastic Finite-Element Analyses of Constraint Variations in Cracked Bodies," presented at 24th National Symposium on Fracture Mechanics, Galinburg, TN, 1992.

[26] Shivakumar, K. N. and Newman, J. C., Jr., "ZIP3D - An Elastic and Elastic-Plastic Finite-Element Analysis Program for Cracked Bodies," NASA TM 102753, Nov. 1990.

[27] Hudson, C. M., "Effect of Stress Ratio on Fatigue-Crack Growth in 7075-T6 and 2024-T3 Aluminum-Alloy Specimens," NASA TN D-5390, August 1969.

[28] Phillips, E. P., "The Influence of Crack Closure on Fatigue Crack Growth Thresholds in 2024-T3 Aluminum Alloy," Mechanics of Fatigue Crack Closure, ASTM STP 982, 1988, pp. 505-515.

[29] Newman, J. C., Jr., "A Nonlinear Fracture Mechanics Approach to the Growth of Small Cracks," Behaviour of Short Cracks in Airframe Components, AGARD CP-328, 1982, pp. 6.1-6.26.

[30] Schijve, J., Jacobs, F. A. and Tromp, P. J., "Crack Propagation in Aluminum Alloy Sheet Materials under Flight Simulation Loading," NLR-TR 68117 U, National Aerospace Laboratory, Dec. 1968.

[31] Schijve, J., Jacobs, F. A. and Tromp, P. J., "Fatigue Crack Growth in Aluminum Alloy Sheet Materials under Flight Simulation Loading - Effects of Design Stress Level and Loading Frequency," NLR-TR 72018 U, National Aerospace Laboratory, 1972.

[32] Newman, J. C., Jr., Wu, X. R., Swain, M. H., Zhao, W., Phillips, E. P. and Ding, C. F., "Small-Crack Growth Behavior in High-Strength Aluminum Alloys - A NASA/CAE Cooperative Program," 18th Congress International Council of Aeronautical Sciences, Beijing, China, Sept. 21-25, 1992.

[33] Dill, H. D. and Saff, C. R., "Spectrum Crack Growth Prediction Method based on Crack Surface Displacement and Contact Analyses," Fatigue Crack Growth under Spectrum Loading, ASTM STP 595, 1976, pp. 306-319.

[34] Fuhring, H. and Seeger, T., "Structural Memory of Cracked Components under Irregular Loading," Fracture Mechanics, ASTM STP 677, 1979, pp. 144-167.

[35] de Koning, A. U. and Liefing, G., "Analysis of Crack Opening Behavior by Application of a Discretized Strip Yield Model," Mechanics of Fatigue Crack Closure, ASTM STP 982, 1988, pp. 437-458.

[36] Wanhill, R. J. H., "Flight Simulation Fatigue Crack Propagation Evaluation of Candidate Lower Wing Skin Materials with Particular Consideration of Spectrum Truncation," NLR TR 77092 U, July 1977.

[37] Wanhill, R. J. H., "Gust Spectrum Fatigue Crack growth in Candidate Skin Materials," Fatigue of Engineering Materials and Structures, Vol. 1, 1979, pp. 5-19.

[38] ProvoKluit, J. C., "Significance of Crack Closure for Crack Growth in 7075-T6 and 2024-T3 Al-Alloys under Flight Simulation Loading with Different Truncation Levels (in Dutch)", Thesis Delft University of Technology, 1978.

[39] Newman, J. C, Jr. and Dawicke, D. S., "Prediction of Fatigue-Crack Growth in a High-Strength Aluminum Alloy Under Variable-Amplitude Loading," Advances in Fracture Research, ICF7, Houston, TX, 1989, pp. 945-952.

[40] Chermahini, R. G., Shivakumar, K. N. and Newman, J. C., Jr., "Three-Dimensional Finite-Element Simulation of Fatigue Crack Growth and Closure," Mechanics of Fatigue Crack Closure, ASTM STP 982, 1988, pp. 398-413.

Table 1.-Baseline ΔK_{eff}-Rate Relations.

2024-T3 Alclad (a)		7075-T6 Clad (b)	
ΔK_{eff} MPa-$\sqrt{m}$	dc/dN m/cycle	ΔK_{eff} MPa-$\sqrt{m}$	dc/dN m/cycle
1.05	1.0E-11	0.9	1.0E-11
1.05	1.0E-10	1.25	1.0E-09
2.2	2.0E-09	3.2	1.0E-08
4.1	1.0E-08	5.0	1.15E-07
7.6	1.0E-07	8.0	5.0E-07
10.7	4.0E-07	14.0	2.0E-06
17.0	3.0E-06	17.5	1.0E-05
35.0	1.0E-04	28.5	1.0E-04

(a) B = 2 mm and σ_0 = 420 MPa.

(b) B = 2 mm and σ_0 = 520 MPa.

Table 2.-Variable-Constraint Regime.

Material	B mm	dc/dN m/cycle	α
2024-T3 Alclad	1.6	1.0E-07	2.0
		1.0E-06	1.0
2024-T3 Alclad	2.0	1.0E-07	2.0
		1.5E-06	1.0
2024-T3 Alclad	3.1	1.0E-07	2.0
		3.5E-06	1.0
7075-T6 Clad	2.0	5.0E-07	2.0
		7.0E-06	1.15

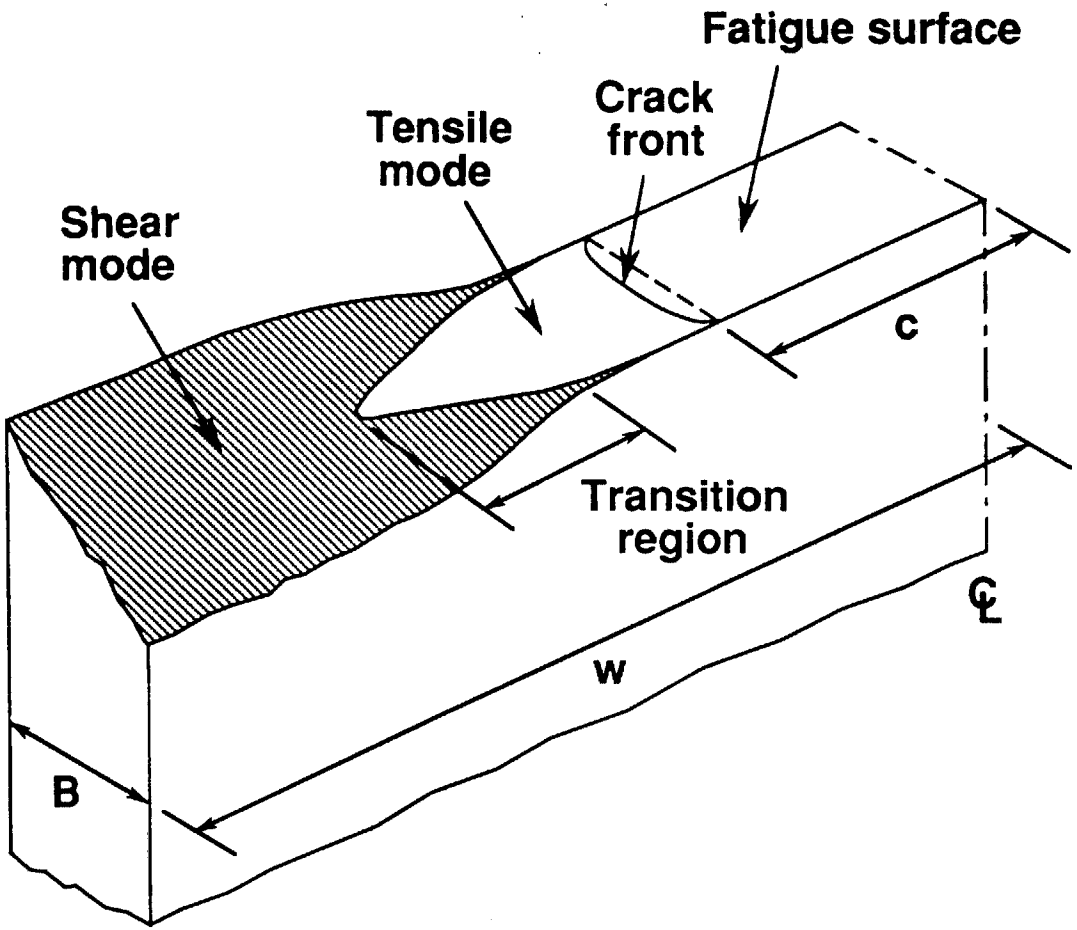

Figure 1. Fatigue crack surface with transition from tensile to shear mode.

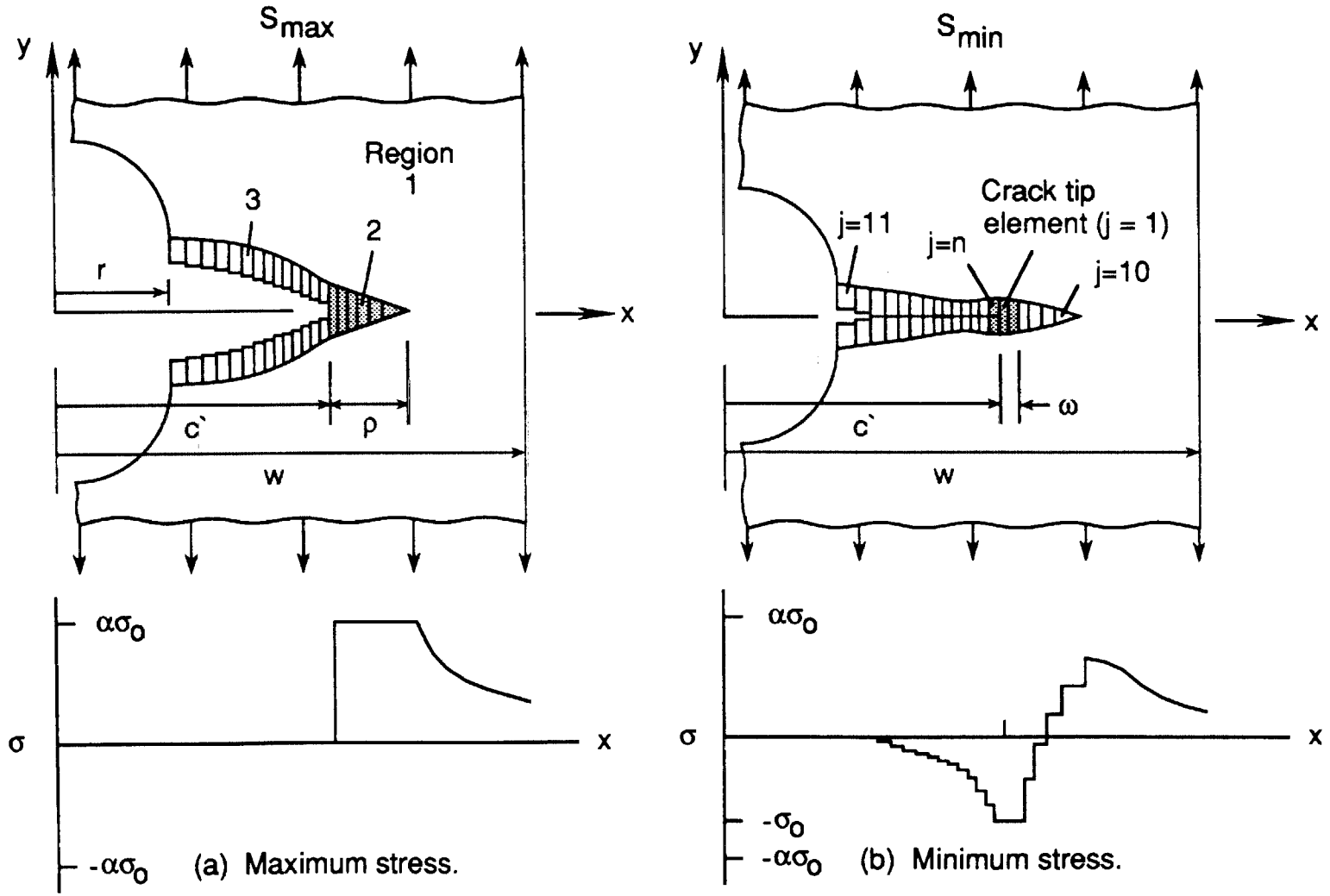

Figure 2. Schematic of analytical crack-closure model under cyclic loading.

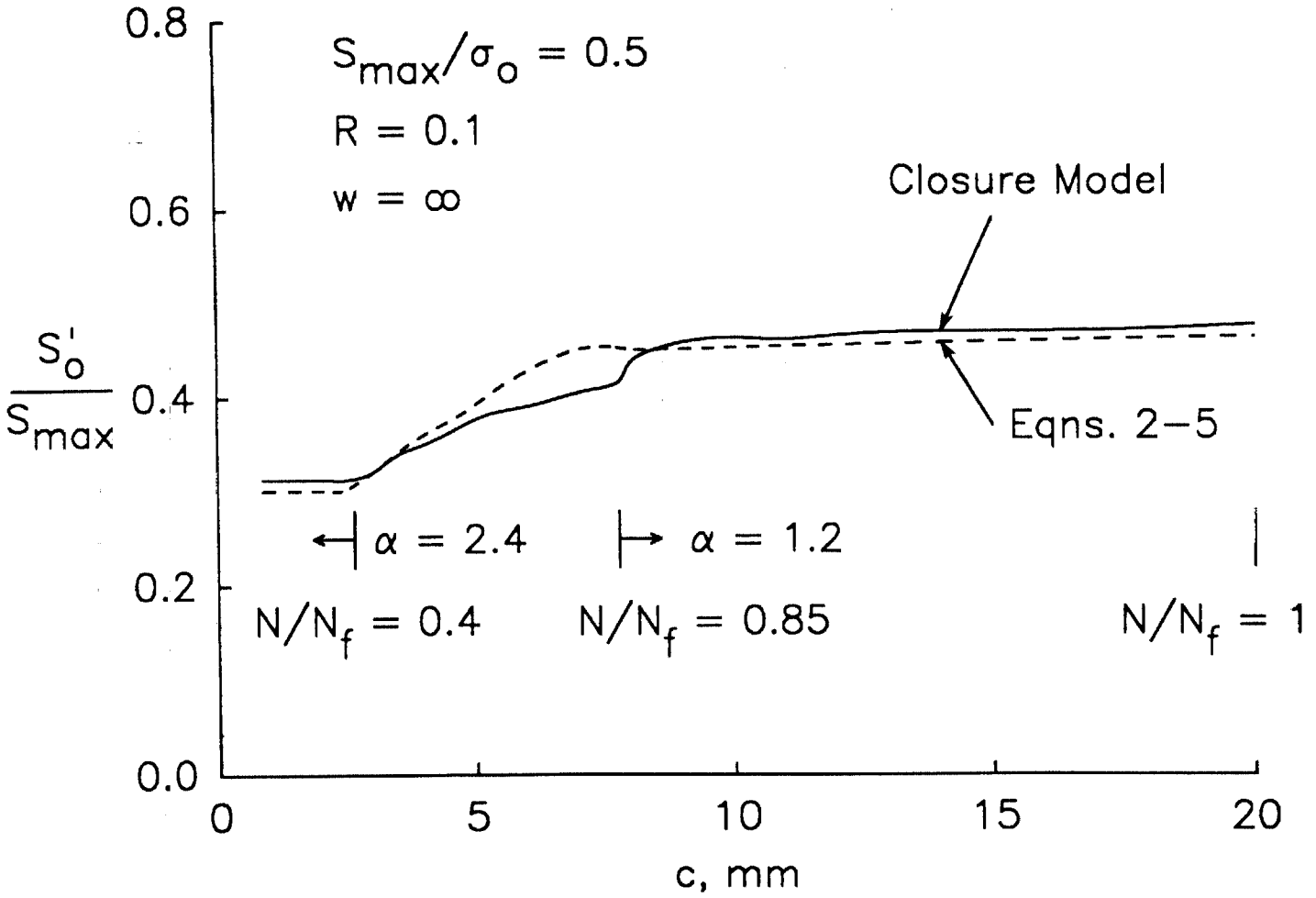

Figure 3. Comparison of calculated crack-opening stresses from model and equations during regions of constant and changing constraint.

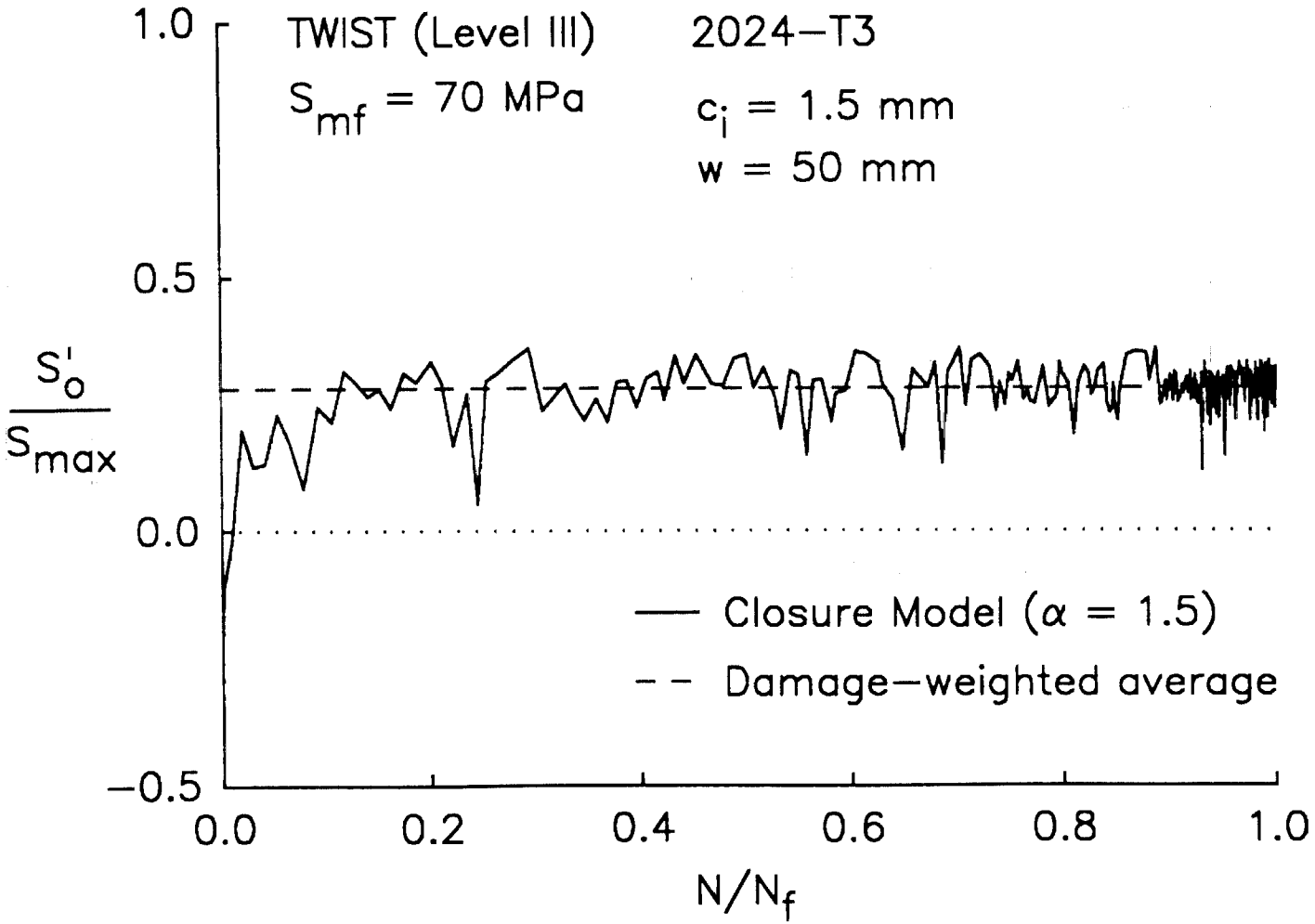

Figure 4. Calculated crack-opening stresses from model and damage-weighted average for constant constraint factor under TWIST loading.

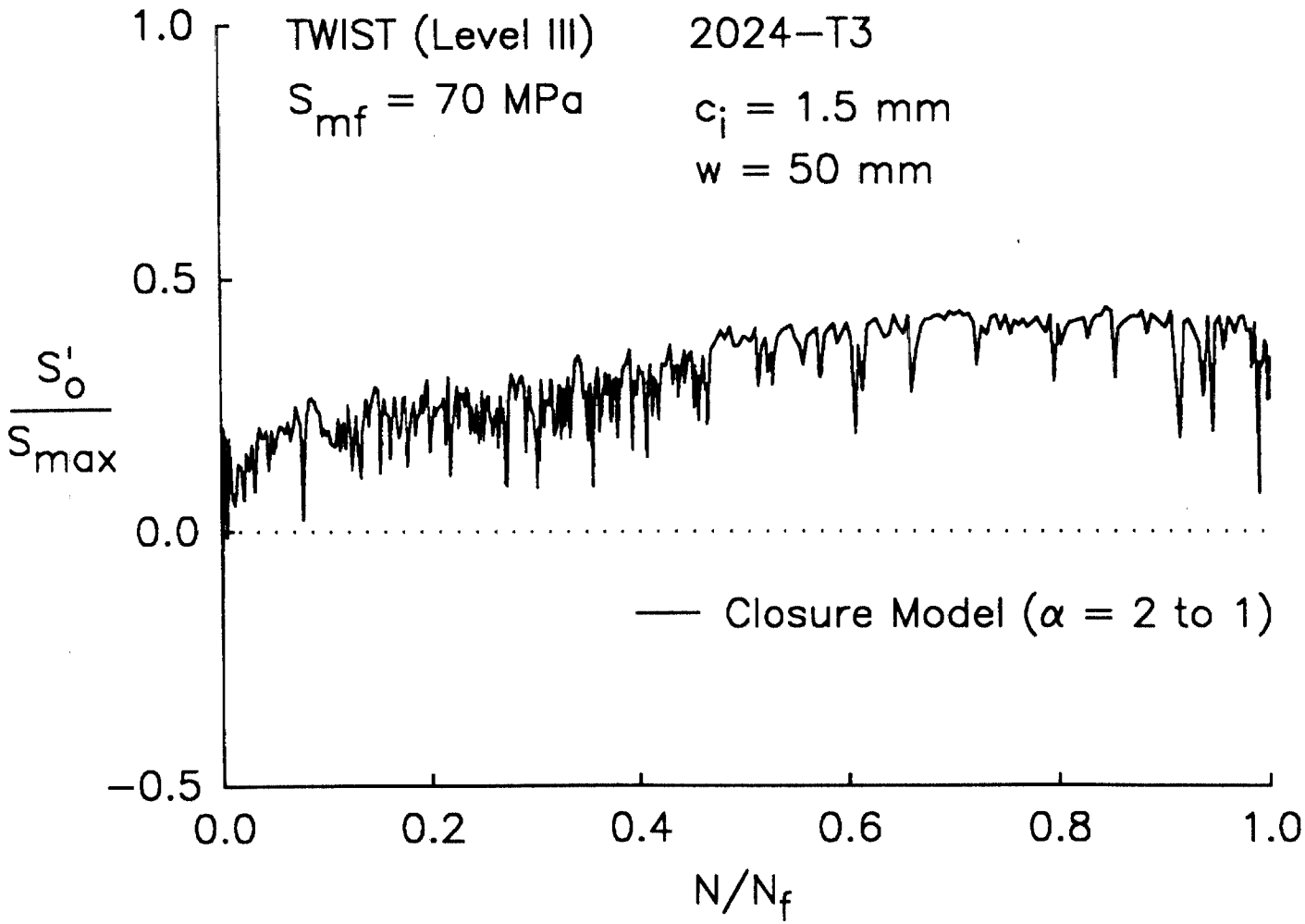

Figure 5. Calculated crack-opening stresses from model for an assumed constraint variation under TWIST loading.

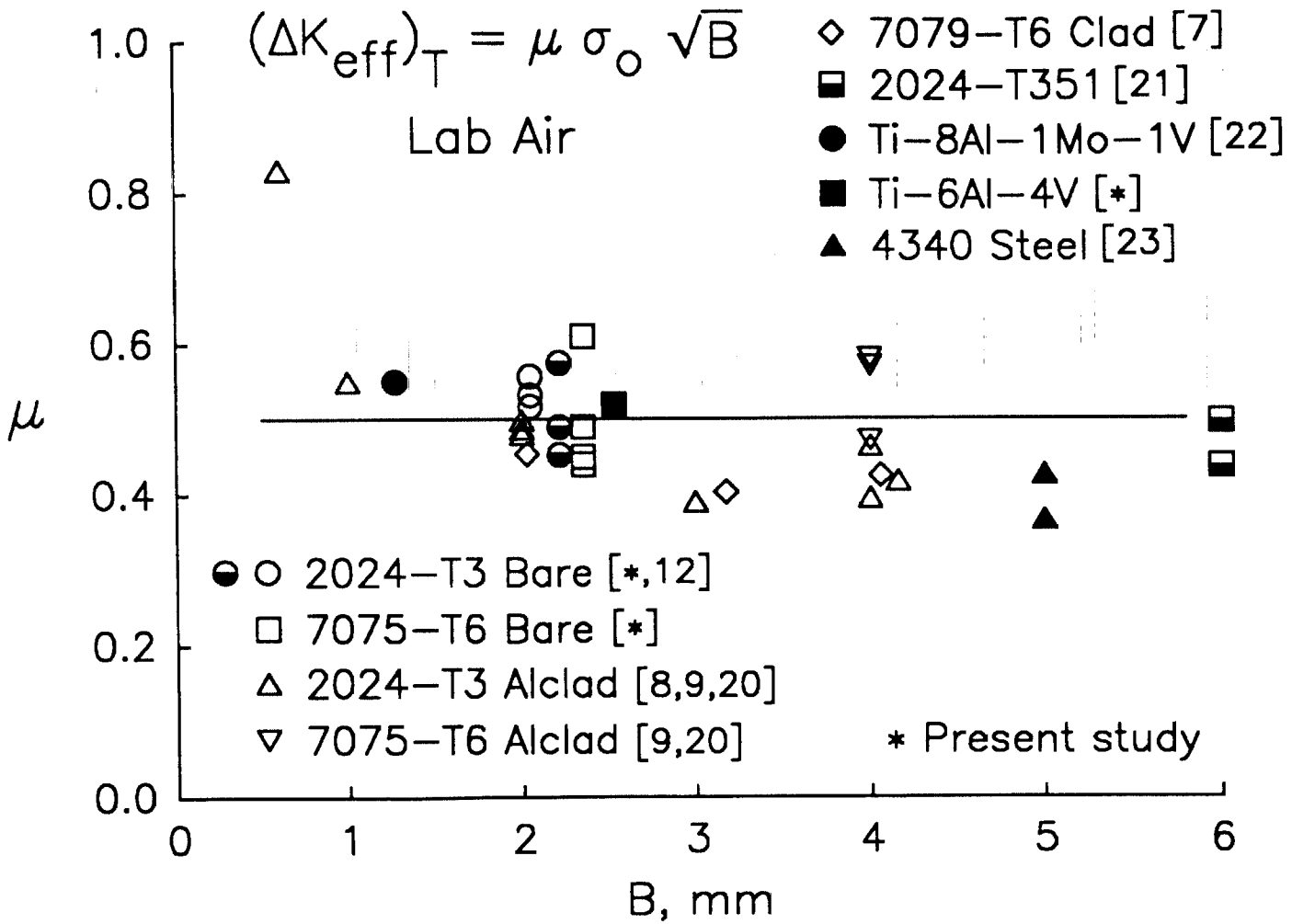

Figure 6. Transitional coefficient for various materials under laboratory air conditions.

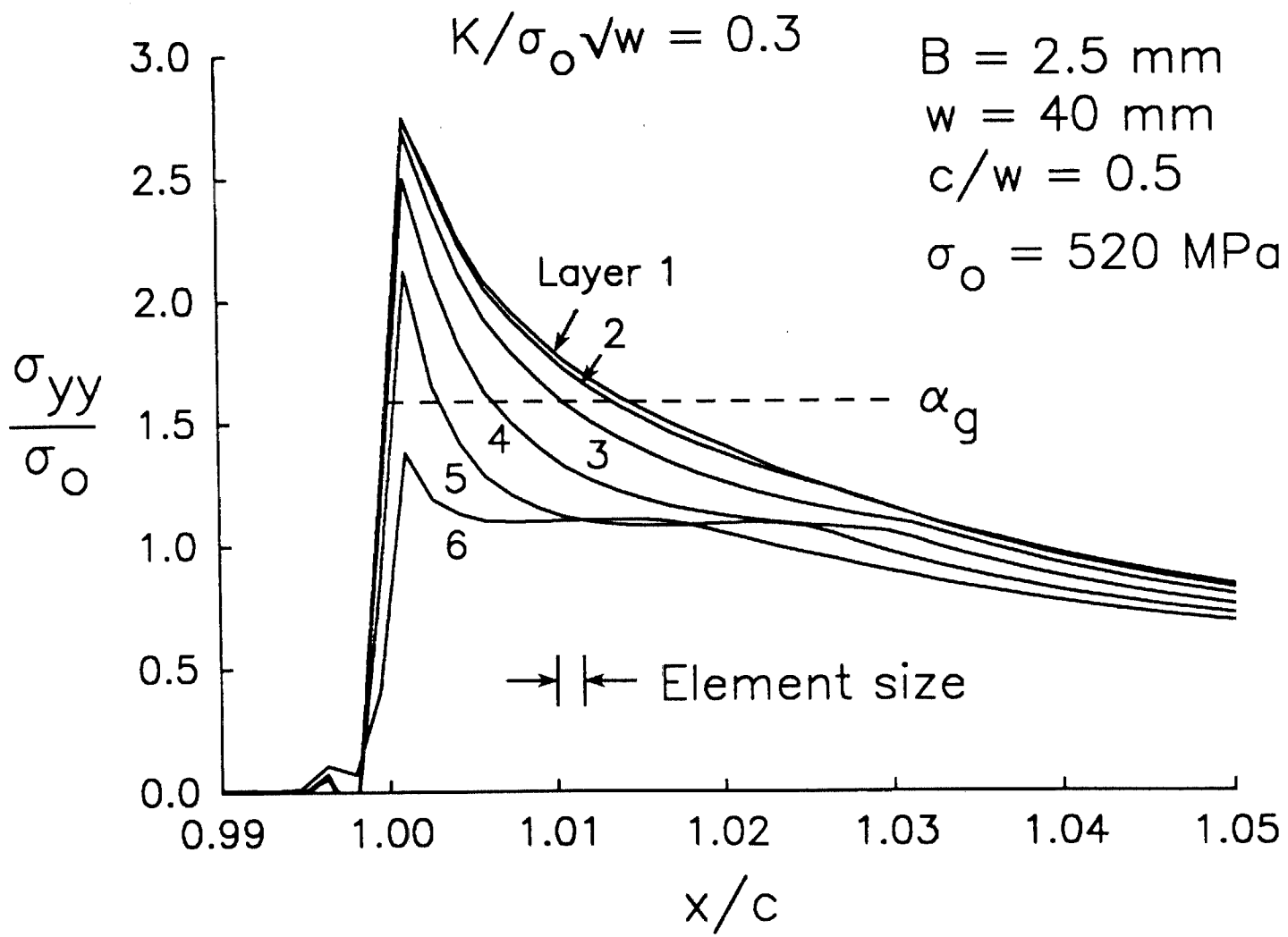

Figure 7. Comparison of normal stress distribution and global constraint factor at crack front for thin sheet under monotonic loading.

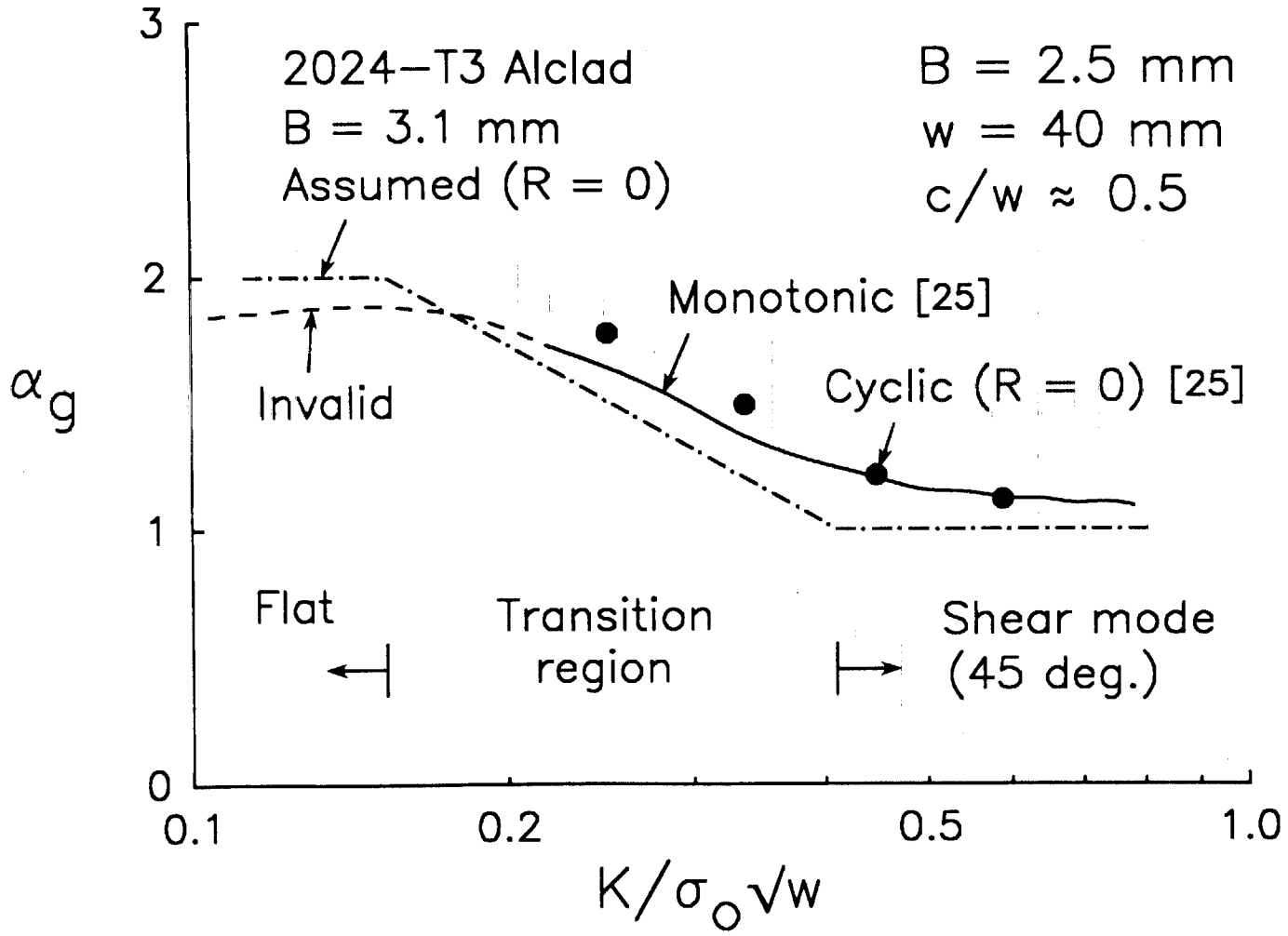

Figure 8. Comparison of global constraint factor from 3D finite-element analyses with an assumed constraint variation for a thin sheet.

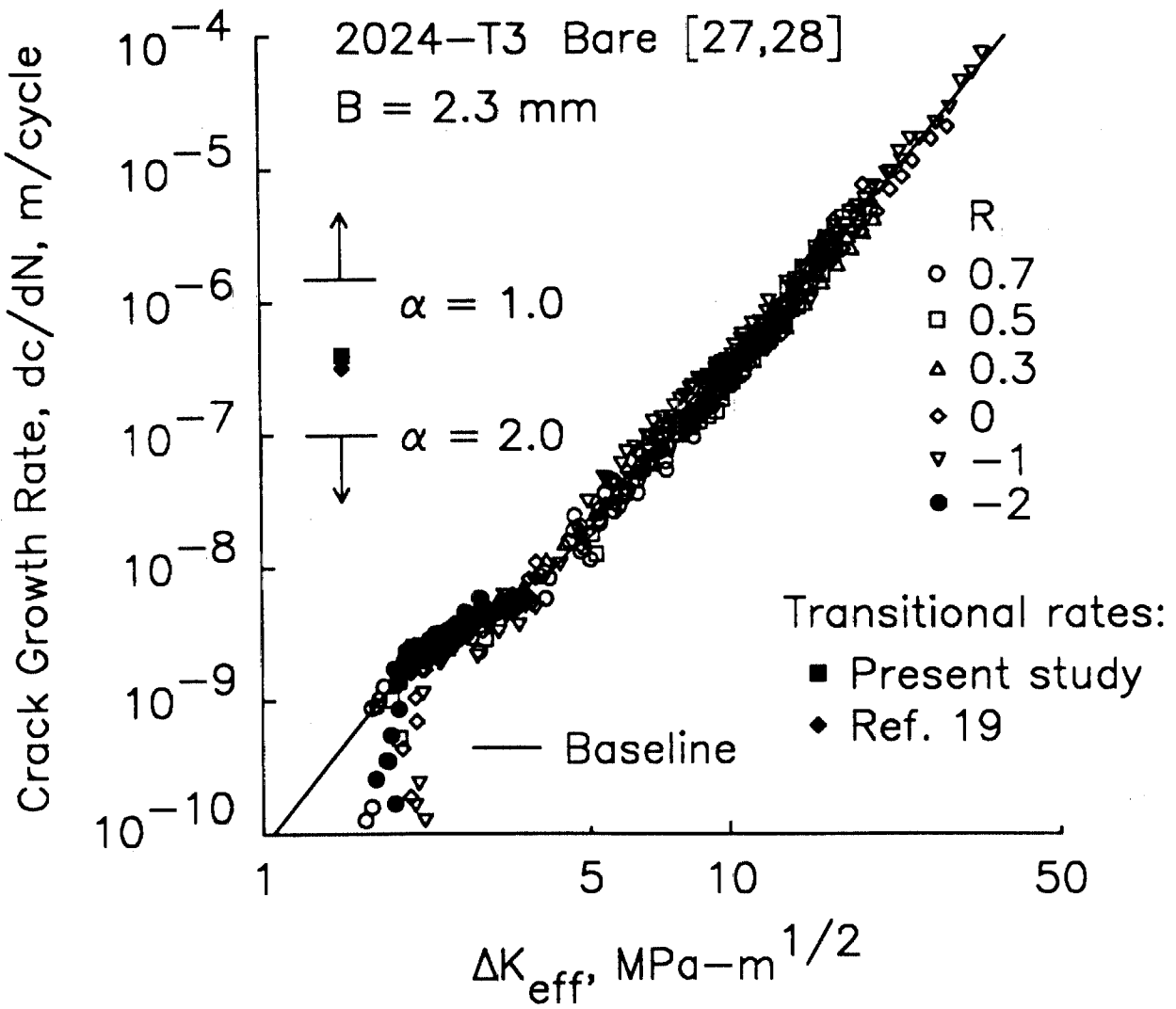

Figure 9. Effective stress-intensity factor range against crack-growth rate for 2024-T3 Bare aluminum alloy.

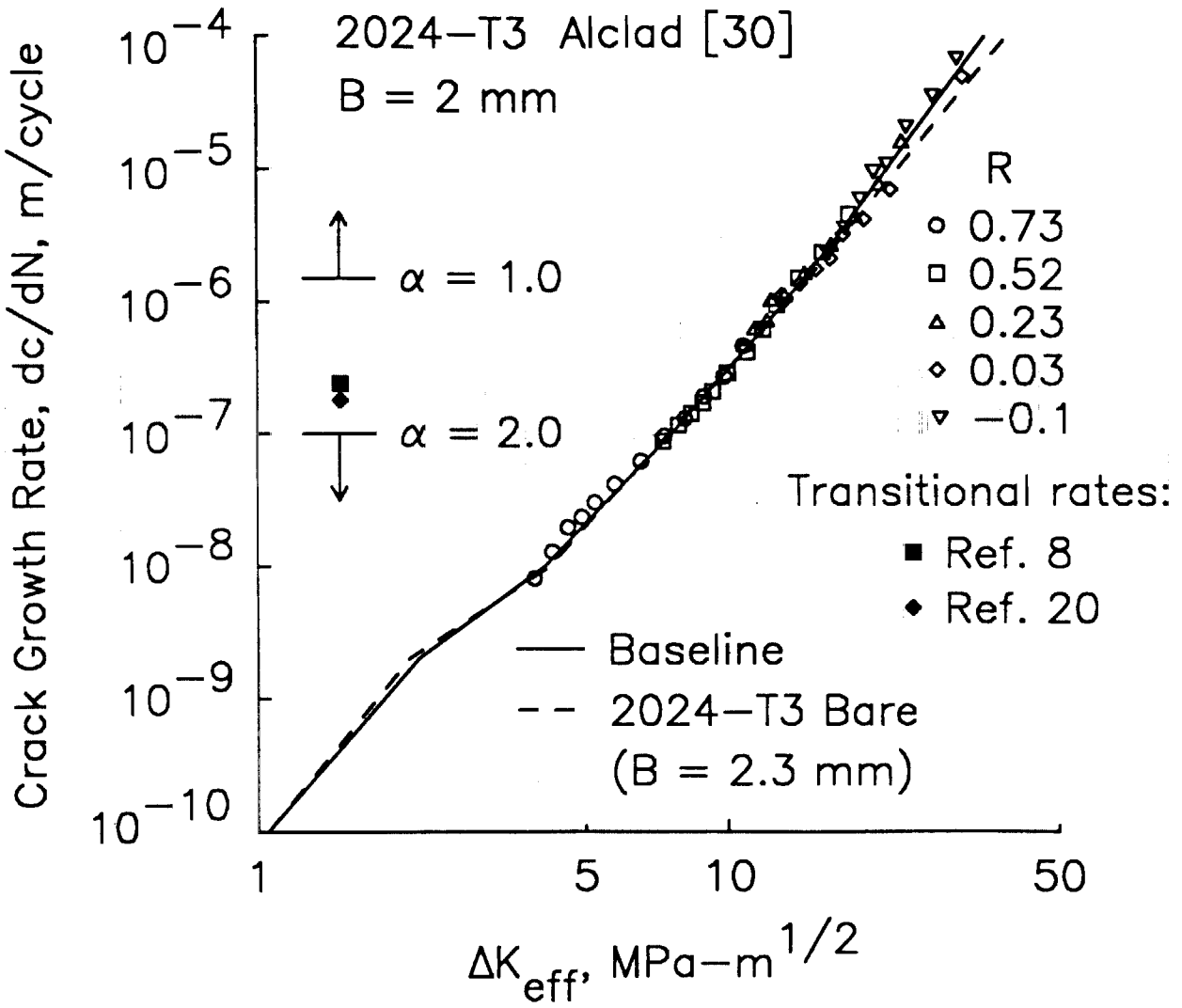

Figure 10. Effective stress-intensity factor range against crack-growth rate for 2024-T3 Alclad aluminum alloy.

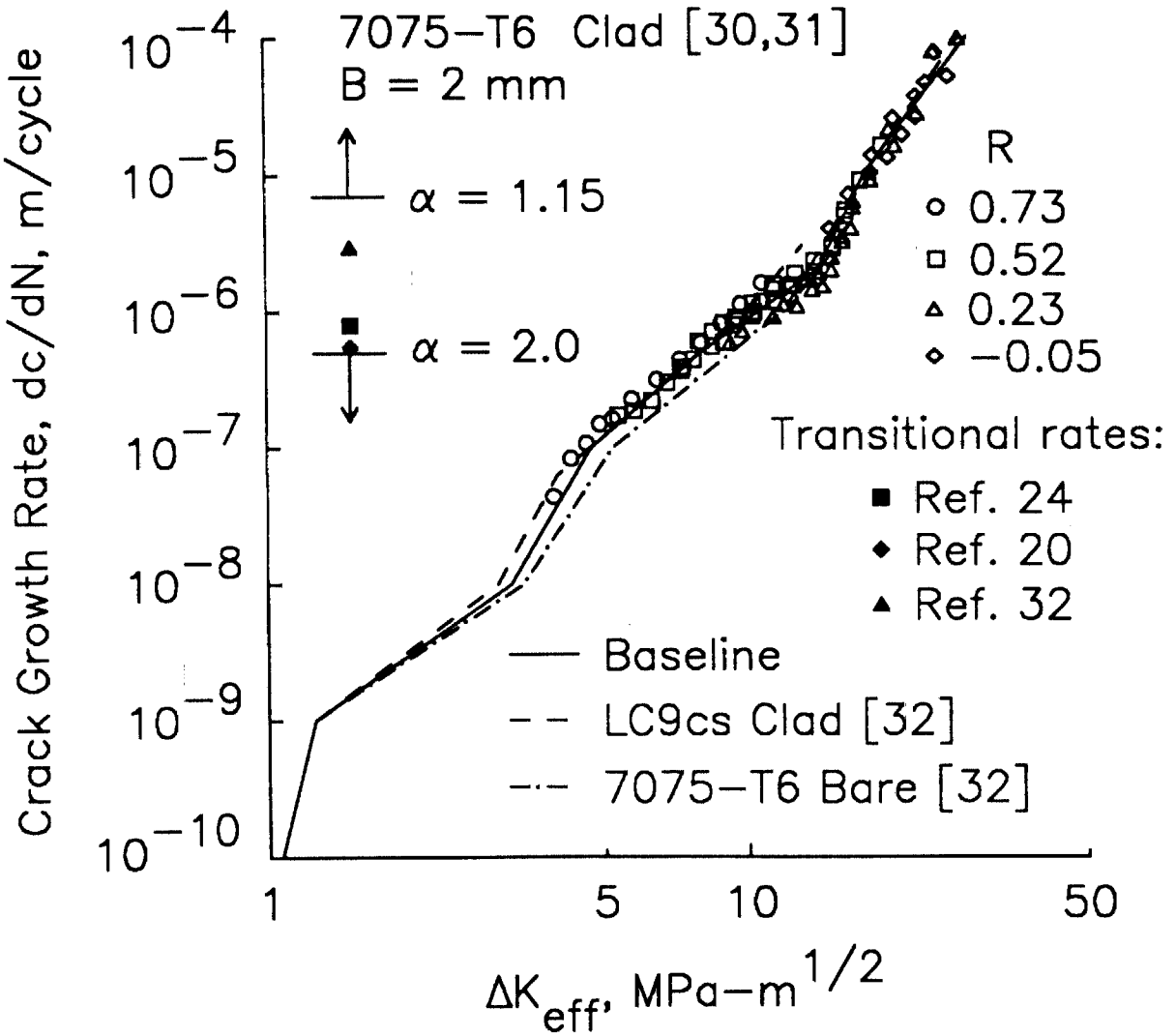

Figure 11. Effective stress-intensity factor range against crack-growth rate for 7075-T6 Clad aluminum alloy.

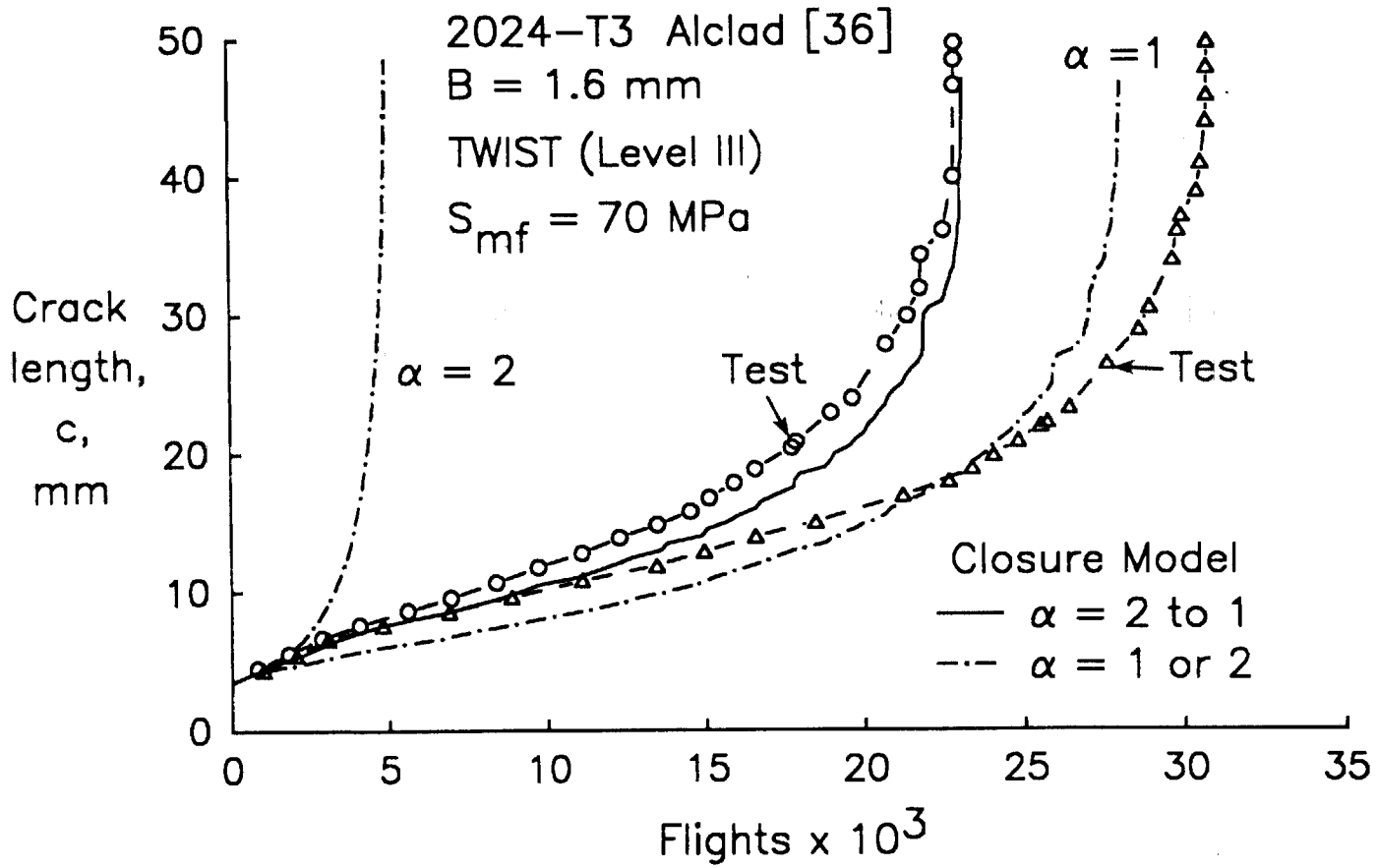

Figure 12. Comparison of measured and calculated crack-length-against-flights for 1.6 mm-thick aluminum alloy under TWIST loading.

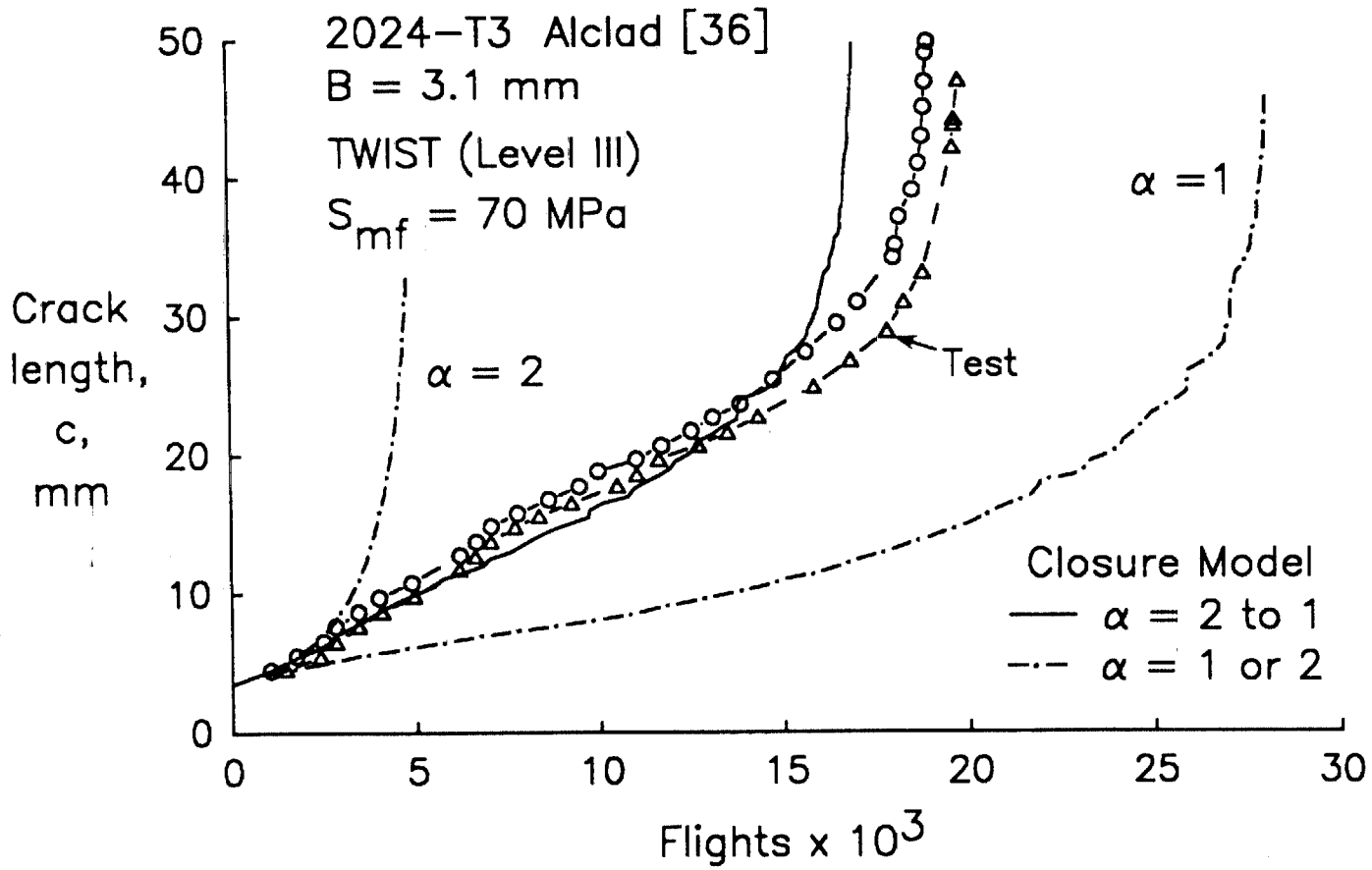

Figure 13. Comparison of measured and calculated crack-length-against-flights for 3.1 mm-thick aluminum alloy under TWIST loading.

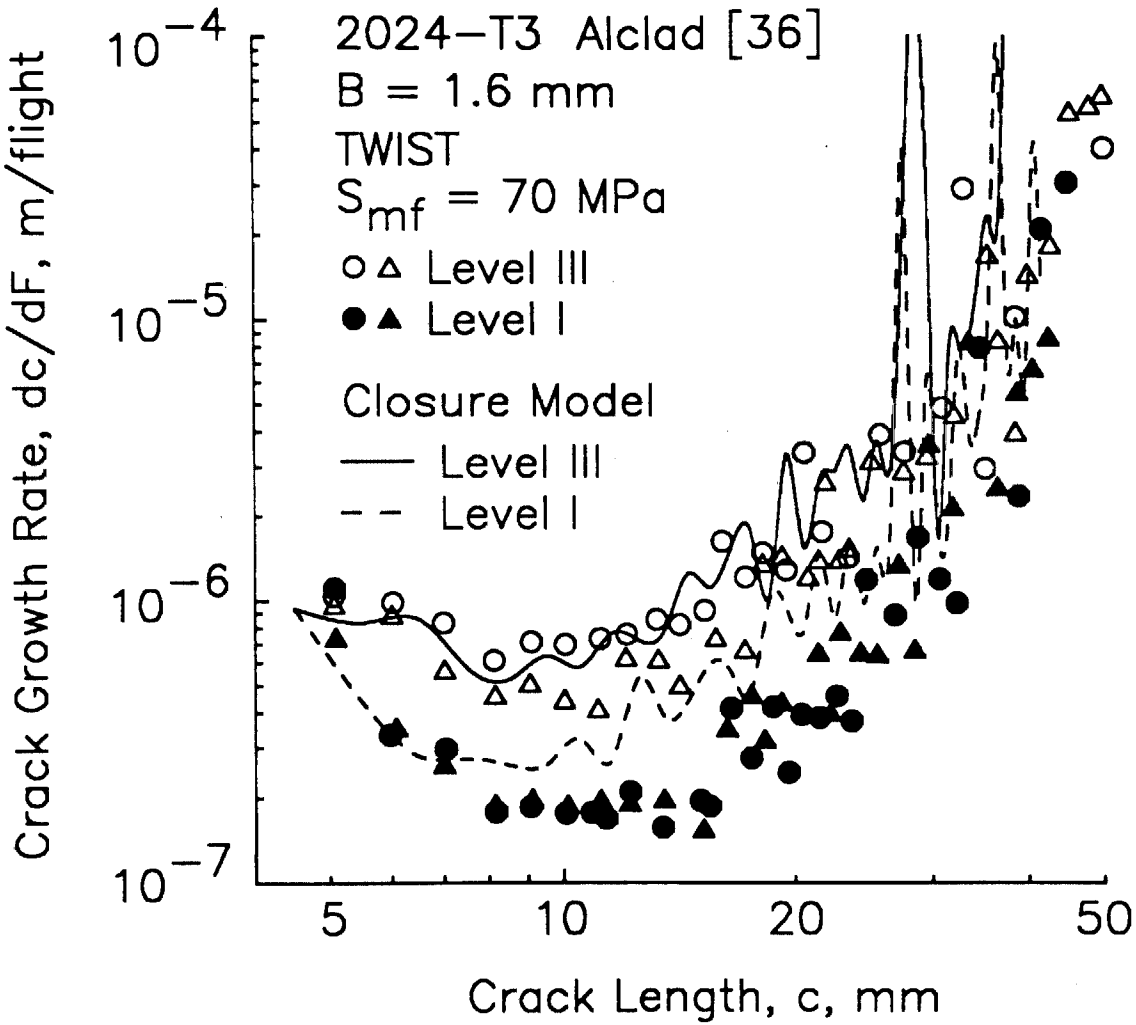

Figure 14. Comparison of measured and calculated rates for 1.6 mm-thick aluminum alloy under TWIST loading clipped at Levels I and III.

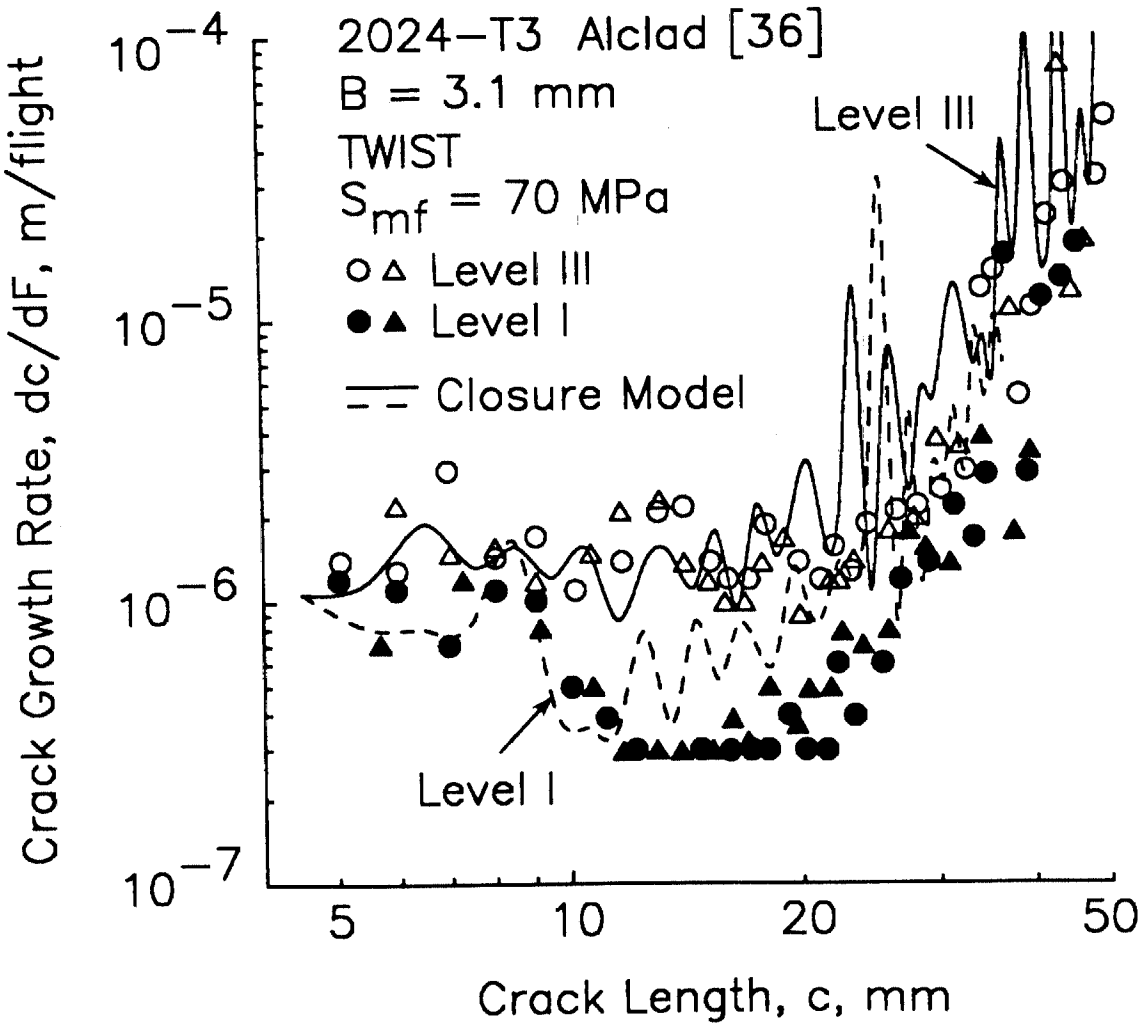

Figure 15. Comparison of measured and calculated rates for 3.1 mm-thick aluminum alloy under TWIST loading clipped at Levels I and III.

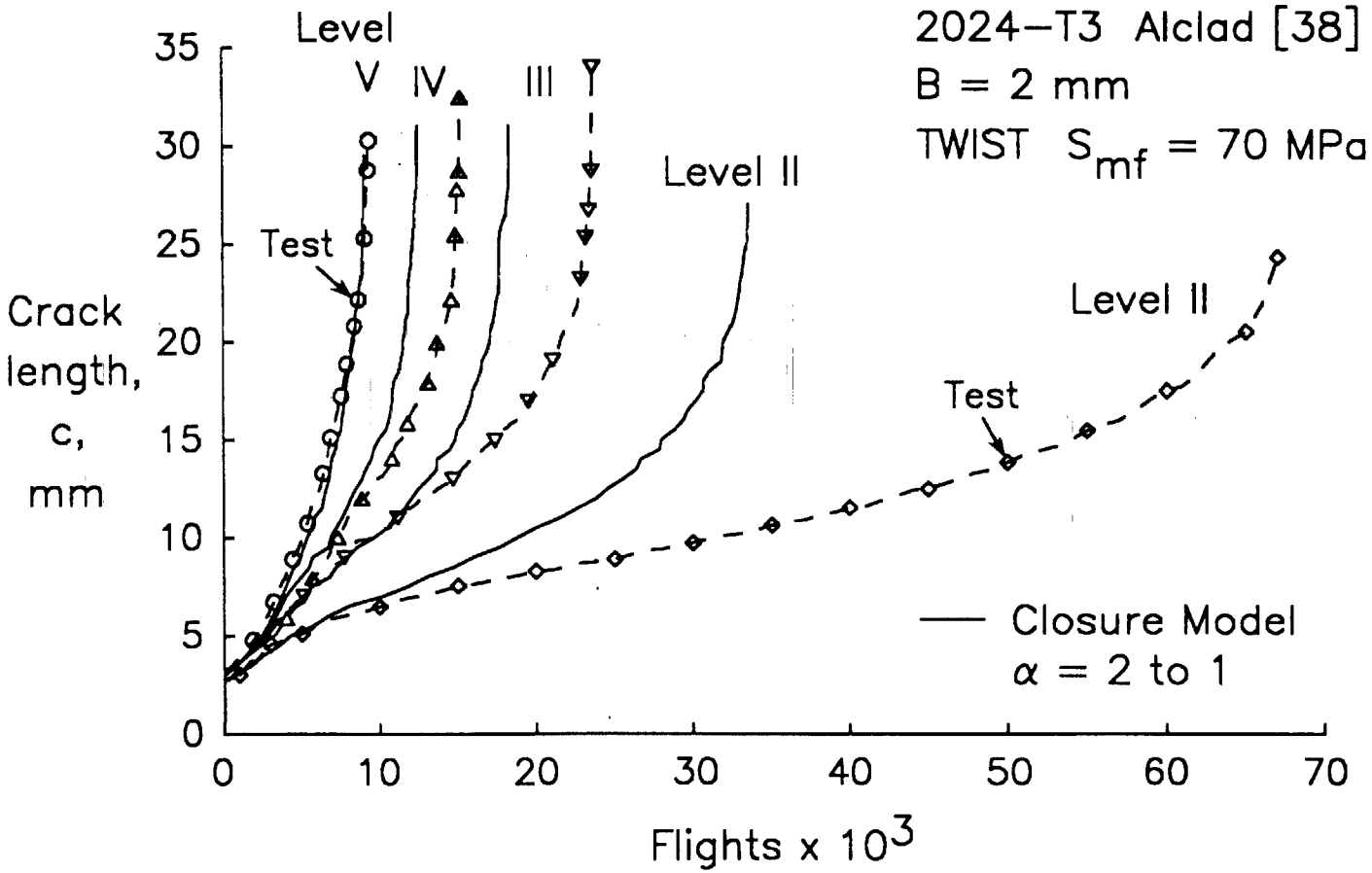

Figure 16. Comparison of measured and calculated crack-length-against-flights for 2024-T3 Alclad under TWIST loading (Levels II to V).

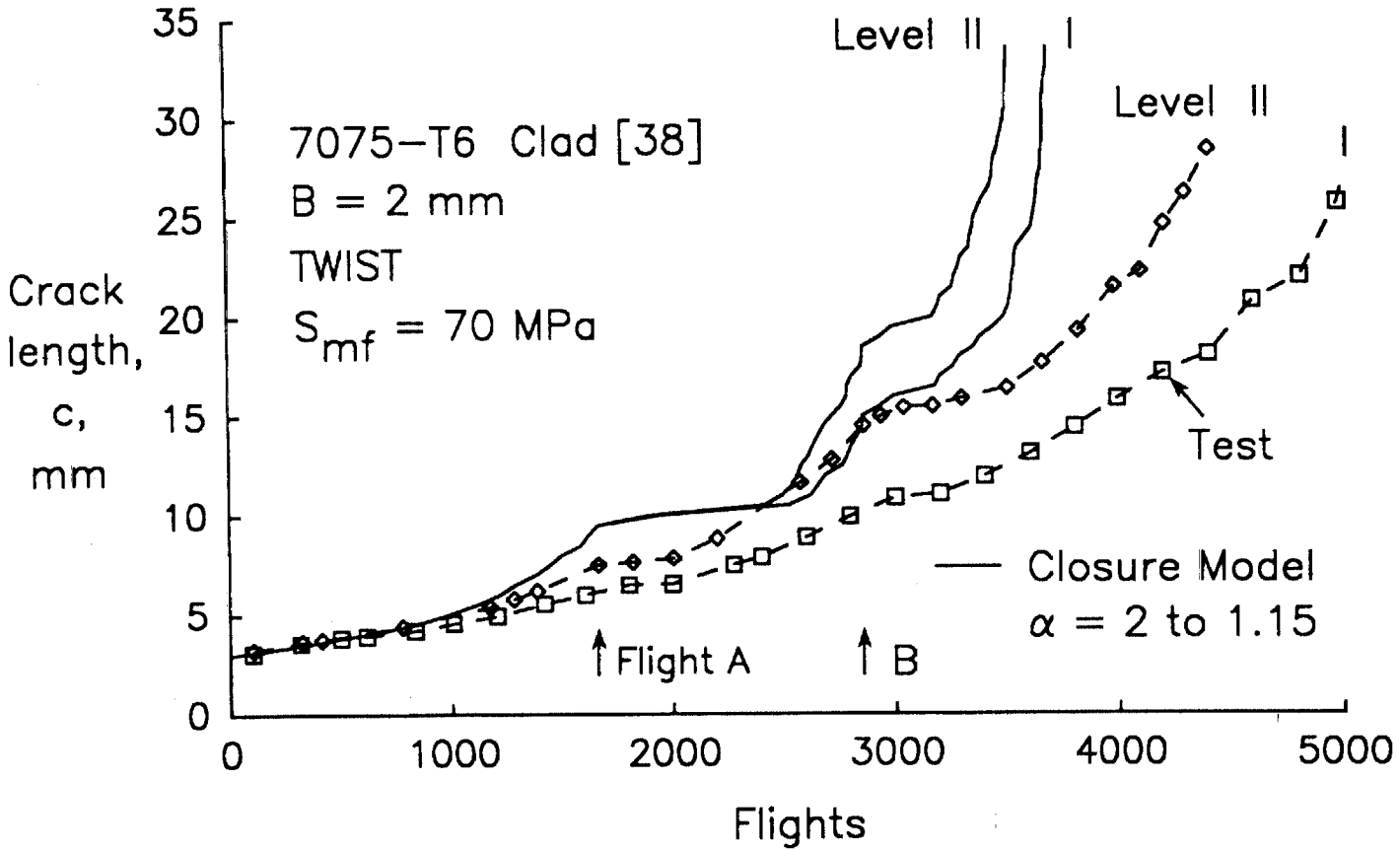

Figure 17(a). Comparison of measured and calculated crack-length-against-flights for 7075-T6 Clad under TWIST loading (Levels I and II).

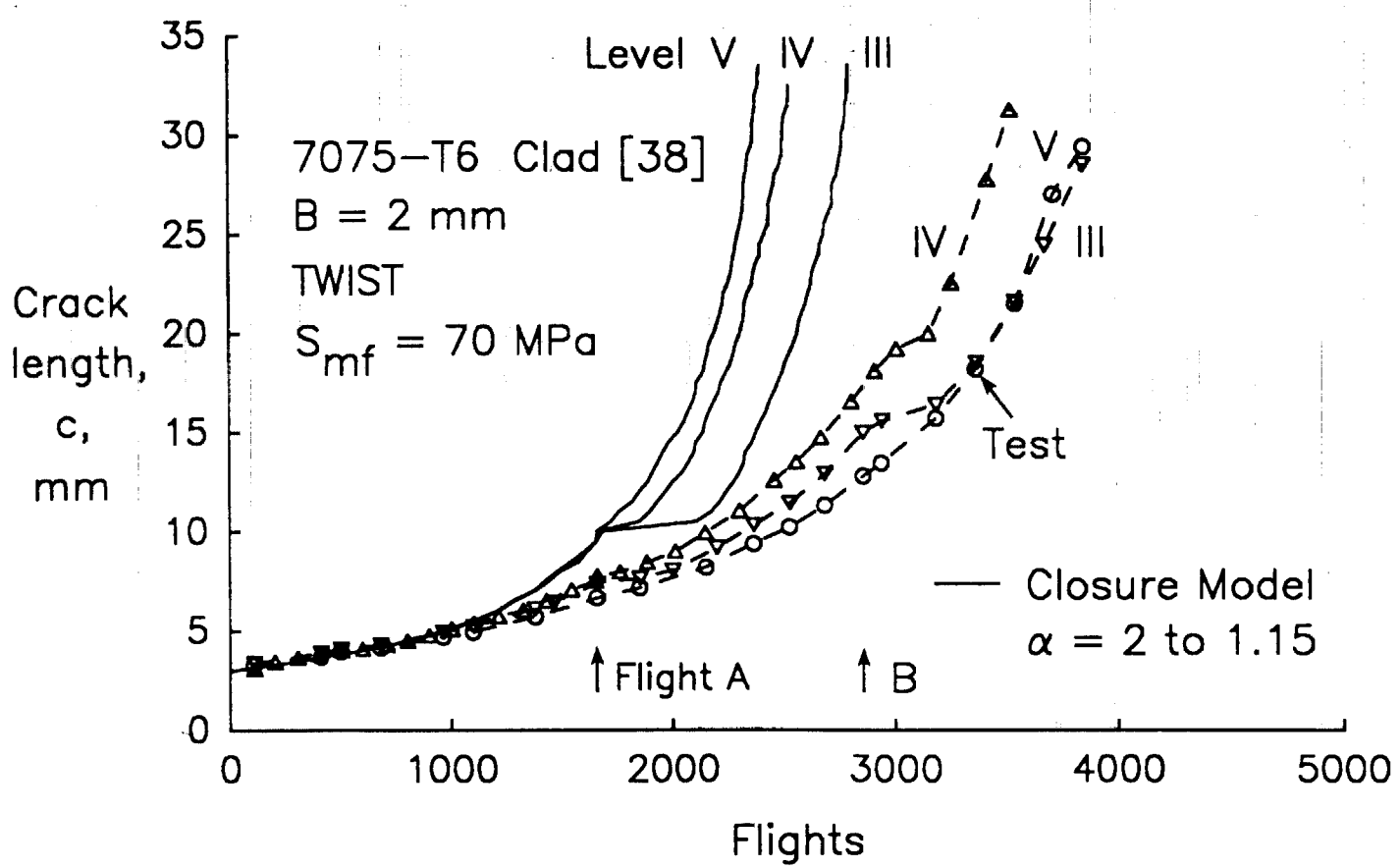

Figure 17(b). Comparison of measured and calculated crack-length-against-flights for 7075-T6 Clad under TWIST loading (Levels III to V).

REPORT DOCUMENTATION PAGE

Form Approved
OMB No 0704-0188

Public reporting burden for this collection of information is estimated to average 1 hour per response, including the time for reviewing instructions, searching existing data sources, gathering and maintaining the data needed, and completing and reviewing the collection of information. Send comments regarding this burden estimate or any other aspect of this collection of information, including suggestions for reducing this burden, to Washington Headquarters Services, Directorate for information Operations and Reports, 1215 Jefferson Davis Highway, Suite 1204, Arlington, VA 22202-4302, and to the Office of Management and Budget, Paperwork Reduction Project (0704-0188), Washington, DC 20503

1. AGENCY USE ONLY *(Leave blank)*	2. REPORT DATE	3. REPORT TYPE AND DATES COVERED
	September 1992	Technical Memorandum

4. TITLE AND SUBTITLE
Effects of Constraint on Crack Growth Under Aircraft Spectrum Loading

5. FUNDING NUMBERS
WU 538-02-10-01

6. AUTHOR(S)

7. PERFORMING ORGANIZATION NAME(S) AND ADDRESS(ES)
NASA Langley Research Center
Hampton, VA 23681-0001

8. PERFORMING ORGANIZATION REPORT NUMBER

9. SPONSORING / MONITORING AGENCY NAME(S) AND ADDRESS(ES)
National Aeronautics and Space Administration
Washington, DC 20546-0001

10. SPONSORING / MONITORING AGENCY REPORT NUMBER
NASA TM-107677

11. SUPPLEMENTARY NOTES

12a. DISTRIBUTION / AVAILABILITY STATEMENT
Unclassified - Unlimited

Subject Category 39

12b. DISTRIBUTION CODE

13. ABSTRACT *(Maximum 200 words)*

The objective of this paper is to study the effects of constraint on fatigue crack growth under aircraft spectrum loading. A plasticity-induced crack-closure model that accounts for constraint variations during the transition from flat-to-slant crack growth was used to correlate crack-growth rate data under constant-amplitude loading and to calculate crack growth under simulated aircraft spectrum loading. The model was applied to several thin-sheet aluminum alloy materials. Under laboratory air conditions, the transition was shown to be related to the size of the cyclic plastic zone based on the effective stress-intensity factor range for several sheet materials and thicknesses. Results from three-dimensional, elastic-plastic, finite-element analyses of a flat, straight-through crack in a thin-sheet aluminum alloy specimen showed a constraint loss similar to that assumed in the model. Using test data and the closure model, the location of the constraint-loss regime in terms of growth rate and the value of the constraint factor at these rates were determined by trial and error. The model was then used to calculate crack growth under the TWIST spectrum. The calculated results agreed reasonably well with test data. In general, the model predicted shorter crack-growth lives than tests under the TWIST spectrum by about 40 percent. For the TWIST spectrum clipped at Level III, the calculated lives were within about 20 percent. The results demonstrated that constraint variations, especially for thin-sheet alloys, should be accounted for to predict crack growth under typical aircraft spectra.

14. SUBJECT TERMS	15. NUMBER OF PAGES
Stress-intensity factor plasticity; Crack closure; TWIST; Finite-element analyses	48
	16. PRICE CODE: A03

17. SECURITY CLASSIFICATION OF REPORT	18. SECURITY CLASSIFICATION OF THIS PAGE	19. SECURITY CLASSIFICATION OF ABSTRACT	20. LIMITATION OF ABSTRACT
Unclassified	Unclassified		